

Rethinking Early Stopping: Refine, Then Calibrate

Eugène Berta^{1,2} David Holzmüller^{1,2} Michael I. Jordan^{1,3} Francis Bach^{1,2}

Abstract

Machine learning classifiers often produce probabilistic predictions that are critical for accurate and interpretable decision-making in various domains. The quality of these predictions is generally evaluated with proper losses like cross-entropy, which decompose into two components: *calibration error* assesses general under/overconfidence, while *refinement error* measures the ability to distinguish different classes. In this paper, we provide theoretical and empirical evidence that these two errors are not minimized simultaneously during training. Selecting the best training epoch based on validation loss thus leads to a compromise point that is suboptimal for both calibration error and, most importantly, refinement error. To address this, we introduce a new metric for early stopping and hyperparameter tuning that makes it possible to minimize refinement error during training. The calibration error is minimized after training, using standard techniques. Our method integrates seamlessly with any architecture and consistently improves performance across diverse classification tasks.

1. Introduction

Accurate classification lies at the heart of many machine learning applications, from medical diagnosis to autonomous driving systems. Modern classifiers predict not only a class label but also a probability vector reflecting the model’s confidence that the instance belongs to each class. This probabilistic output is critical for downstream decision-making. Despite their widespread use, many machine learning models, especially complex ones such as neural networks, tend to produce poorly calibrated probabilities (Guo et al., 2017), meaning that the predicted confidence does not align with real-world probabilities.

This issue has mostly been considered through the lens of post-hoc calibration, which consists in adjusting the pre-

¹INRIA, Paris ²Ecole Normale Supérieure, PSL Research University, Paris ³University of California, Berkeley.
Correspondence to: Eugène Berta <eugene.berta@inria.fr>.

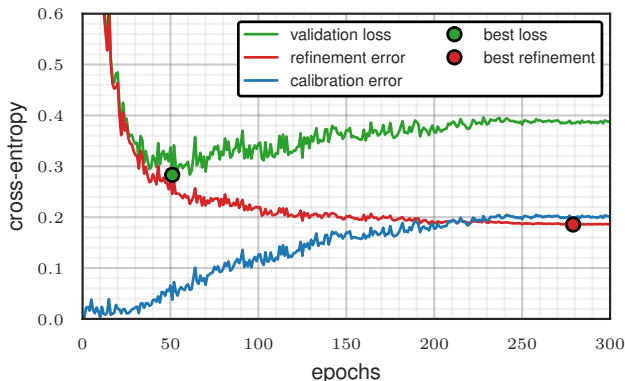


Figure 1: **Calibration-refinement decomposition during training.** We plot the calibration and refinement terms of the validation cross-entropy—measured with our estimator from Section 3—for a ResNet18 on the CIFAR10 dataset (training details available in Appendix F). Calibration and refinement are not minimized simultaneously, the loss minimizer is thus suboptimal for both errors.

dicted probabilities after training, using a small held-out portion of the dataset. An overlooked aspect of the problem is that the calibration error contributes to the total loss of a classifier (Bröcker, 2009). In Figure 1 we plot the decomposition of the classification loss (here cross-entropy) into calibration error and refinement error during training for a deep neural network. We observe that the two are not minimized simultaneously. The resulting validation loss minimizer thus has a non-zero calibration error and is suboptimal for refinement. This observation reveals that there is room for improvement in the way we train machine learning classifiers.

In Sections 2 and 3 we propose minimizing only the refinement error during training and the calibration error after training. This new paradigm can be used seamlessly with any machine learning model by simply using our new refinement estimator, provided in the package github.com/dholzmuller/probmetrics, as a stopping metric. In Section 4, we present empirical evidence of the loss reduction achieved across various problems. In Sections 5 and 6, we study logistic regression on a binary Gaussian data model, demonstrating that the problem exists even in simple settings and that our method minimizes both refinement and calibration errors.

2. Calibration-Refinement decomposition

We begin by overviewing the decomposition of proper losses into calibration and refinement errors. We also present a new variational formulation of this decomposition that allows a reinterpretation of refinement as the loss after optimal post-processing.

Notation. Consider classification with k classes. Let Δ_k denote the probability simplex $\{p \in [0, 1]^k \mid \mathbf{1}^\top p = 1\}$ and $\mathcal{Y}_k \subset \Delta_k$ the space of one-hot encoded labels $y \in \{0, 1\}^k$ with $y_i = 1$ if the true class is i and $y_i = 0$ otherwise. Assume we have a random variable $X \in \mathcal{X}$ (the feature vector), such that there is an unknown joint probability distribution \mathcal{D} on (X, Y) . We make probabilistic predictions $p \in \Delta_k$ on the value of the true label Y using a statistical model $f : \mathbb{R}^p \rightarrow \Delta_k$.

2.1. Proper loss decomposition

We evaluate predictions with a loss function $\ell : \Delta_k \times \mathcal{Y}_k \rightarrow \mathbb{R}_+$. ℓ is a nonnegative function of p and y such that $\ell(p, y)$ assesses the quality of prediction p for label y . Well-known examples include the Brier score $\ell(p, y) = \|y - p\|_2^2$ and the cross-entropy (logloss) $\ell(p, y) = -\sum_{i=1}^k y_i \log(p_i)$. Suppose the label y is sampled from a distribution $q \in \Delta_k$. We use the same notation to denote the expected loss obtained when making prediction p : $\ell(p, q) = \mathbb{E}_{y \sim q}[\ell(p, y)]$. A natural requirement is that $\ell(\cdot, q)$ is minimized (only) in q , in this case, ℓ is called (strictly) proper.

Let $C = \mathbb{E}_{\mathcal{D}}[Y|f(X)]$, the random variable measuring the expectation of Y given the prediction. Proper losses satisfy the following decomposition of the risk (Bröcker, 2009):

$$\mathbb{E}[\ell(f(X), Y)] = \mathbb{E}[d_\ell(f(X), C)] + \mathbb{E}[e_\ell(C)], \quad (1)$$

where $d_\ell(p, q) := \ell(p, q) - \ell(q, q)$ and $e_\ell(q) := \ell(q, q)$ are respectively the divergence and entropy associated with ℓ (we refer to these as ℓ -divergence and ℓ -entropy). For different choices of classification loss, we recover well-known entropy and divergence functions.

Proper loss ℓ	Divergence d_ℓ	Entropy e_ℓ
Logloss $-\sum_i y_i \log(p_i)$	KL divergence $\sum_i q_i \log \frac{q_i}{p_i}$	Shannon entropy $-\sum_i q_i \log q_i$
Brier score $\ y - p\ _2^2$	Squared distance $\ p - q\ _2^2$	Gini index $\sum_i q_i(1 - q_i)$

The first term in the decomposition (1) is the *calibration error* $\mathcal{K}_\ell(f)$ associated with ℓ . The second term, denoted $\mathcal{R}_\ell(f)$, is the *refinement error* for ℓ . Refinement error is sometimes further decomposed into the irreducible loss (risk of the optimal classifier f^*), and the grouping loss (Kull & Flach, 2015; Perez-Lebel et al., 2023).

2.2. Calibration error

Calibration has received a lot of attention on its own, not always in the context of the calibration-refinement decomposition. A model f is said to be *calibrated* if $f(X) = C$ almost surely. When this is satisfied, for a given prediction $f(X) = p$, the expected outcome $C = \mathbb{E}[Y|f(X)]$ is aligned with p . This is a desirable property in that it makes model predictions interpretable as probabilities that Y belongs to each of the k classes.

Calibration error. Model mis-calibration is thus measured by the expected gap between $f(X)$ and C . The choice of a distance or divergence function d gives rise to different notions of *calibration error*: $\mathcal{K}^{(d)}(f) = \mathbb{E}[d(f(X), C)]$. A popular choice for d is the L^1 distance, resulting in the expected calibration error (ECE, Naeini et al., 2015). Note that when picking the L^2 distance or KL divergence, we recover “proper” calibration errors (Gruber & Buettner, 2022), that appear in the decomposition of the Brier score and the logloss. In practice, the data distribution \mathcal{D} is only known via a finite set of samples $(x_i, y_i)_{1 \leq i \leq n}$ and f makes continuous predictions $f(x_i) \in \Delta_k$. To compute the calibration error, C is often estimated by binning predictions on the simplex, resulting in estimators that are biased and inconsistent (Kumar et al., 2019; Vaicenavicius et al., 2019; Roelofs et al., 2022). In the multi-class case, the curse of dimensionality makes estimation even more difficult. Weaker notions like class-wise or top-label calibration error are often used (Kumar et al., 2019; Kull et al., 2019).

Post hoc calibration. Many machine learning classifiers suffer from calibration issues, which gave rise to a family of techniques known as “post hoc calibration.” These methods reduce calibration error after training using a reserved set of samples \mathcal{C} called a “calibration set.” Among others, isotonic regression and temperature scaling are widely used.

Isotonic regression (IR, Zadrozny & Elkan, 2002) finds the monotonic function g^* that minimizes the risk of $g \circ f$ on the calibration set. It is a popular calibration technique for binary classifiers. The multi-class extensions come with important drawbacks however.

Temperature scaling (TS, Guo et al., 2017) optimizes a scalar parameter β to rescale the log-probabilities. Formally, it learns the function g_{β^*} on the calibration set with

$$\begin{aligned} g_\beta(p) &:= \text{softmax}(\beta \log(p)), \\ \beta^* &:= \operatorname{argmin}_{\beta \in \mathbb{R}_+} \mathcal{L}(\beta), \\ \mathcal{L}(\beta) &:= \sum_{(x,y) \in \mathcal{C}} \ell(g_\beta(f(x)), y). \end{aligned} \quad (2)$$

For neural networks, this comes down to rescaling the last layer by β^* . TS has many advantages: it is efficient, applies

to multi-class problems, does not affect accuracy, and is robust to overfitting since it only has one parameter.

We refer the interested reader to [Silva Filho et al. \(2023\)](#) for a detailed review of calibration. In Appendix A we also take a closer look at the literature on the subject and other related works.

2.3. Refinement error

Given the appeal of calibrated predictions, significant effort has been devoted to estimating and reducing calibration error. The fact that it interacts with another term to form the overall risk of the classifier, however, has received much less attention. This is partly due to the fact that refinement error is little known. So what exactly is refinement?

In decomposition (1), it appears as the expected ℓ -entropy of Y given $f(X)$: $\mathcal{R}_\ell(f) = \mathbb{E}[e_\ell(\mathbb{E}[Y|f(X)])]$. With simple intuition about entropy functions, we see that if Y is fully determined by $f(X)$, $Y|f(X)$ has no entropy and the refinement error is null. In contrast, if $Y|f(X)$ is as random as Y , it is maximal. Refinement error thus quantifies how much of the variability in Y is captured by $f(X)$, with a lower error indicating greater information. Just like classification error, it assesses the ability to distinguish between classes independently of calibration issues like over/under-confidence. It provides a much more comprehensive measure, however, as it considers the entire distribution of $f(X)$ rather than a single discretization. This comes at the cost that, like calibration error, it is much harder to estimate.

2.4. A variational formulation

In Appendix B we introduce novel variational formulations of the terms in decomposition (1), most importantly:

Theorem 2.1. *The refinement error for proper loss ℓ is*

$$\mathcal{R}_\ell(f) = \min_g \mathbb{E}[\ell(g(f(X)), Y)] \quad ,$$

where the minimum is taken over all measurable functions $g : \Delta_k \rightarrow \Delta_k$. It is attained at $g^*(f(X)) = \mathbb{E}[Y|f(X)]$.

Calibration error evaluates how much the population risk can be reduced by optimally re-labeling the original forecasts. This optimal relabeling is given by the calibrated score $C = \mathbb{E}[Y|f(X)]$. This is quite intuitive: such re-labeling sets the calibration error to zero, leaving only the refinement term in the risk decomposition (1). Refinement error thus measures the remaining risk after optimal re-labeling, which corresponds to the risk of the calibrated scores. This new variational formulation reveals that refinement error can be estimated using the risk after post-hoc calibration.

3. Our method: refinement-based stopping

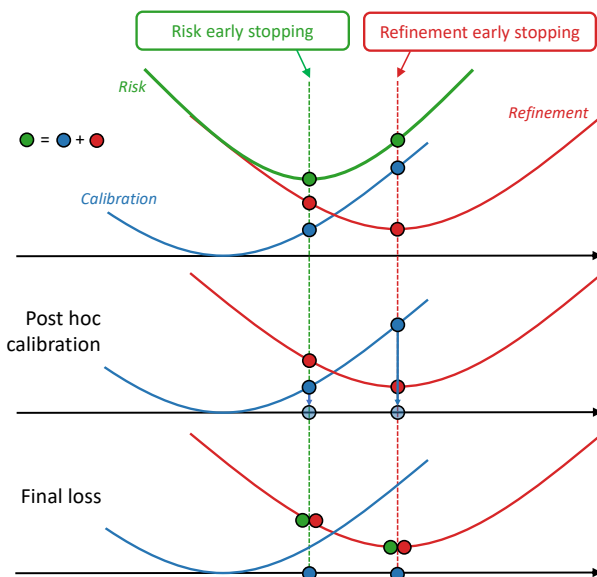


Figure 2: risk-based versus refinement-based early stopping, before and after post hoc calibration. Dots denote risk (green), refinement (red) and calibration (blue) errors.

3.1. refinement-based early stopping: the intuition

Two distinct minimizers. Minimizing the risk of a classifier comes down to minimizing simultaneously refinement and calibration errors. Empirically, these two errors are not minimized simultaneously during training, as in Figure 1. One possible scenario is that the training set becomes well separated, forcing the model to make very confident predictions to keep training calibration error small. In case of a train-test generalization gap, the model becomes overconfident ([Carrell et al., 2022](#)) while refinement error might still decrease. We observe separate minimizers across various machine learning models, whether through iterative training or when tuning a regularization parameter. In Section 6, we analyze this phenomenon theoretically for high-dimensional logistic regression, showing it appears even in very simple settings. The consequence is that risk-based early stopping finds a compromise point between two conflicting objectives: calibration error minimization and refinement error minimization. This corroborates the widely recognized observation that many models are poorly calibrated after training ([Guo et al., 2017](#)).

Refine, then calibrate. The question that arises is: how do we get a model optimal for both calibration and refinement? In general, strictly increasing post hoc calibration techniques like TS leaves refinement unchanged. [Berta et al. \(2024\)](#) showed that binary IR preserves the ROC convex hull, a proxy for refinement. Given that calibration error

is minimized after training, with no impact on refinement, we argue that training should be dedicated to the latter only. We propose selecting the best epoch based on validation refinement error instead of validation loss as a new training paradigm for machine learning classifiers. As illustrated in Figure 2 this procedure leads to smaller loss after post-hoc calibration. Compared with the standard paradigm that minimizes both refinement and calibration during training, we propose *refining* during training, then *calibrating* post hoc.

Early stopping	Training minimizes	Post hoc minimizes
Risk	Cal. + Ref.	Cal.
Refinement	Ref.	Cal.

3.2. Refinement-based stopping made practical

Refinement estimation. As discussed earlier, calibration error estimators are biased, inconsistent, and break in the multi-class case. Since refinement is risk minus calibration, these issues carry over to refinement estimation. One could circumvent this by using proxies like validation accuracy. Theorem 2.1 provides a better alternative: refinement error equals risk after optimal relabeling $g^* \circ f$. We thus need to estimate how small the validation risk can get by re-labeling predictions. Since the validation set $(x_i, y_i)_{1 \leq i \leq n}$ is finite, minimizing over all measurable functions $g : \Delta_k \rightarrow \Delta_k$ would lead to drastic overfitting. However, given a class of functions \mathcal{G} that we intend to use for post hoc calibration, we can estimate refinement error by solving:

$$\hat{\mathcal{R}}_\ell(f) = \min_{g \in \mathcal{G}} \frac{1}{n} \sum_{i=1}^n \ell(g(f(x_i)), y_i)$$

after every epoch. This comes down to early stopping based on validation “loss after post hoc calibration,” which is a biased estimator of refinement error. Compared with Theorem 2.1, we limit ourselves to functions in class \mathcal{G} . A trade-off arises vis-a-vis the size of \mathcal{G} . The larger the class the less biased our estimator but the more prone we are to overfitting the validation set, resulting in poor estimation of the true refinement error. For our method to work, we need to choose a small class \mathcal{G} that comes as close as possible to the optimal re-mapping $g^*(f) = \mathbb{E}[Y|f(X)]$.

TS-refinement for neural nets. We call TS-refinement the estimator obtained when \mathcal{G} is the class of functions generated by temperature scaling. It is parametrized by a single scalar parameter, seriously limiting the capacity to over-fit the validation set. Moreover, TS is very effective at reducing the calibration error of neural networks (however large it is) while leaving refinement unchanged. This is supported by a plethora of empirical evidence (Guo et al., 2017; Wang et al., 2021). We demonstrate in Section 5

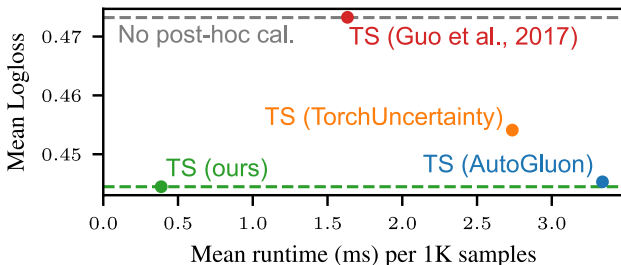


Figure 3: **Runtime versus mean benchmark scores of different TS implementations.** Runtimes are averaged over validation sets with 10K+ samples. Evaluation is on XGBoost models trained with default parameters, using the epoch with the best validation accuracy.

that under assumptions on the logit distribution, the optimal re-mapping g^* is attained by TS, making TS-refinement an unbiased estimator. In practice, when training a neural network, we recommend selecting the best epoch in terms of validation loss after temperature scaling. Going back to the example in Figure 1, this procedure would select a later epoch (red dot), for which validation loss (green curve) is higher but validation loss after TS (red curve) is smaller. Since we were to use TS for post hoc calibration anyway, this simple procedure guarantees a smaller validation risk.

Improving TS implementations. Using TS-refinement for early stopping requires a fast and robust temperature-scaling implementation. Surveying existing codebases made it clear that there is significant room for improvement in terms of both speed and performance. For the logloss, the objective $\mathcal{L}(\beta)$ in equation (2) is convex. Existing implementations apply L-BFGS (Liu & Nocedal, 1989) to optimize $\mathcal{L}(1/T)$, which is unimodal but nonconvex. Additionally, the step-size choice for L-BFGS sometimes led to suboptimal performance. Instead, since \mathcal{L}' is increasing by convexity of \mathcal{L} , we propose using bisection to find a zero of \mathcal{L}' . Figure 3 shows that on the benchmark from Section 4, our implementation achieves lower test loss and is significantly faster than alternatives from Guo et al. (2017), TorchUncertainty, and AutoGluon (Erickson et al., 2020). We provide details in Appendix E.

Other estimators. Our method applies to a wide range of machine learning models. It can help select the best step in any iterative training procedure (e.g, boosting) or the amount of regularization for non-iterative models. Refinement does not have to be estimated with TS-refinement, any proxy available can be selected. For non-neural nets, TS can be less effective. In the binary setting, using risk after isotonic regression (IR-refinement) might be a good option. It is much less biased than TS-refinement since the class \mathcal{G} contains all monotonic functions. The risk of overfitting gets larger however and must be considered carefully.

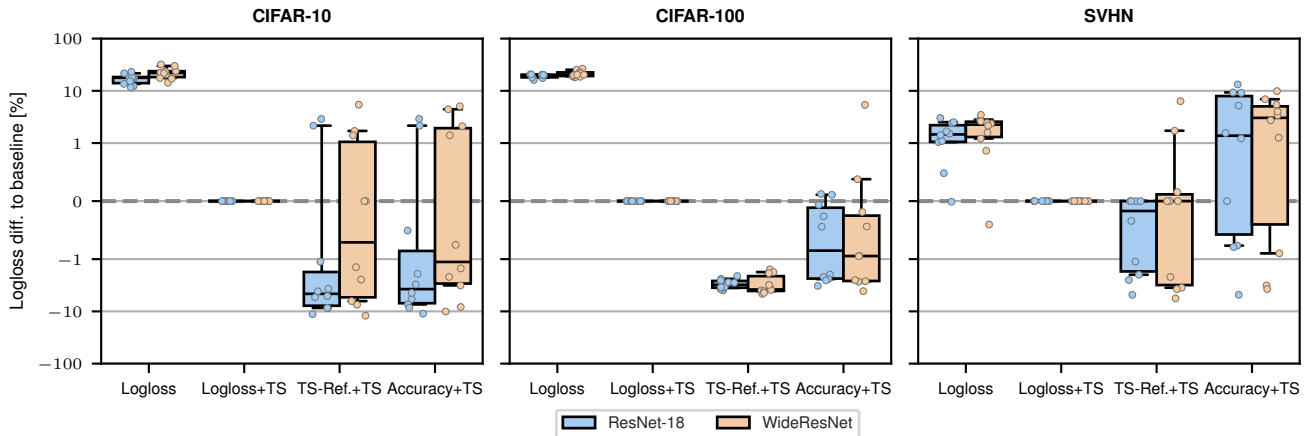


Figure 4: **Relative differences in test logloss (lower is better) between logloss+TS and other procedures on vision datasets.** “+TS” indicates temperature scaling applied to the final model. Each dot represents a training run on one dataset. Box-plots show the 10%, 25%, 50%, 75%, and 90% quantiles. Relative differences (y-axis) are plotted using a log scale.

4. Experiments

Computer Vision. We benchmark our method by training a ResNet-18 (He et al., 2016) and WideResNet (WRN) (Zagoruyko, 2016) on CIFAR-10, CIFAR-100 and SVHN datasets (Krizhevsky et al., 2009; Netzer et al., 2011). We reserve 10% of the training set for validation. We train for 300 epochs using SGD with momentum, weight decay, and a step learning rate scheduler. We use random cropping, horizontal flips, and cutout (DeVries, 2017). For reference, this training procedure allows us to reach 95% accuracy on CIFAR-10 with the ResNet-18 and over 96% with the WRN. We train the models ten times on each dataset. The code to run the benchmark is available at github.com/eugeneberta/RefineThenCalibrate-Vision. On NVIDIA V100 GPUs, the benchmark took around 300 GPU hours to run. We report in Figure 4 the relative differences in test logloss obtained with different training procedures. After early stopping on validation loss (first column), using TS results in significant improvement (second column). Early stopping on TS-refinement instead of validation loss leads to even better results (third column). We also compare with validation accuracy based early stopping (fourth column), another refinement proxy, showing that TS-refinement more consistently yields smaller loss.

We observed empirically that the learning rate scheduler and regularization strength have an influence on the behavior of calibration error during training. This has consequences on the effect observed with our method. In general though, validation TS-refinement remains the best estimator available for test loss after temperature scaling. Brier score, another proper loss, is less sensitive than logloss to sharp variations in calibration error and can be a good alternative for early stopping for practitioners who want to avoid fitting TS every epoch. We refer the interested reader to Appendix F for

details on our training procedure and complete results.

Tabular data, where X is a vector of heterogeneous numerical and/or categorical features, is ubiquitous in ML applications. We take 196 binary and multi-class classification datasets from the benchmark by Ye et al. (2024), containing between 1K and 100K samples after subsampling the largest datasets, see Appendix G. We evaluate three methods:

- **XGBoost** (Chen & Guestrin, 2016) is a popular implementation of gradient-boosted decision trees, with strong performance on tabular benchmarks (Grinsztajn et al., 2022). Due to its iterative optimization, early stopping is relevant for XGBoost as well.
- **MLP** is a simple multilayer perceptron, similar to the popular MLP baseline by Gorishniy et al. (2021).
- **RealMLP** (Holzmüller et al., 2024) is a recent state-of-the-art deep learning model for tabular data (Ye et al., 2024), improving the standard MLP in many aspects.

For each dataset, we report the mean loss over five random splits into 64% training, 16% validation, and 20% test data. For each split, we run 30 random hyperparameter configurations and select the one with the best validation score. The validation set is also used for stopping and post-hoc calibration. Computations took around 40 hours on a 32-core CPU (for XGBoost) and four RTX 3090 GPUs (for NNs).

Figure 5 shows the results on datasets with at least 10K samples. Generally, we observe that TS as well as stopping/tuning on TS-Refinement helps on most datasets, while stopping on accuracy often yields poor logloss even after TS. Our extended analysis in Appendix G shows that results are more noisy and unclear for small or easy datasets. However, stopping on TS-Refinement frequently yields better accuracy and AUC than stopping on logloss, and hence strikes an excellent balance between different metrics.

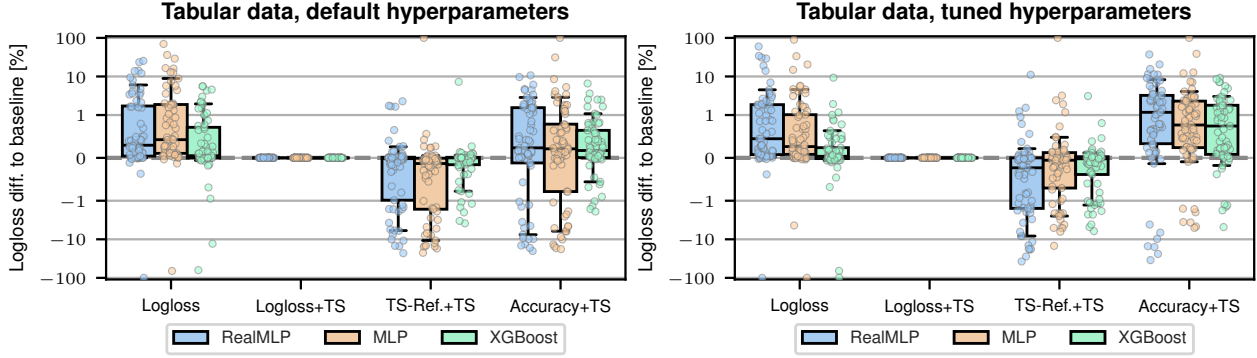


Figure 5: **Relative differences in test logloss (lower is better) between logloss+TS and other procedures on tabular datasets.** “+TS” indicates temperature scaling applied to the final model. Each dot represents one dataset from Ye et al. (2024), using the 65 datasets with 10K+ samples. Percentages are clipped to $[-100, 100]$ due to one outlier with almost zero loss. Box-plots show the 10, 25, 50, 75, and 90% quantiles. Relative differences (y-axis) are plotted using a log scale.

5. Decomposition in the Gaussian data model

In this section and the next, we embark on a theoretical analysis that provides insight into the calibration-refinement decomposition. We demonstrate that even with a simple data model and predictor, calibration and refinement errors are not minimized simultaneously. This highlights the relevance of refinement-based early stopping and underscores the broad impact of the problem we address.

We use the following stylized model. Consider the feature and label random variables $X \in \mathbb{R}^p, Y \in \{-1, 1\}$ under the two-class Gaussian model $X \sim \mathcal{N}(\mu, \Sigma)$ if $Y = 1$ and $X \sim \mathcal{N}(-\mu, \Sigma)$ if $Y = -1$ for some mean $\mu \in \mathbb{R}^p$ and covariance $\Sigma \in \mathbb{R}^{p \times p}$. We further assume balanced classes, $\mathbb{P}(Y = 1) = \mathbb{P}(Y = -1) = \frac{1}{2}$. Under this data model, $\mathbb{P}(Y = 1|X = x) = \sigma(w^* \top x)$ with $w^* = 2\Sigma^{-1}\mu$ and $\sigma(x) = \frac{1}{1+e^{-x}}$ denotes the sigmoid function. The sigmoid function’s shape is well suited to describe the posterior probability of Y given X . Note that this holds for any pair $P(X|Y = \pm 1)$ from the same exponential family (Jordan, 1995). Proofs for this section are deferred to Appendix C.

We are interested in the calibration and refinement errors of the linear model $f(x) = \sigma(w \top x)$. The weight vector w can be learned with techniques such as logistic regression or linear discriminant analysis (Fisher, 1936). Denoting $a_w = \langle w, w^* \rangle_\Sigma / \|w\|_\Sigma$ with $\langle w, w^* \rangle_\Sigma = w \top \Sigma w^*$ and $\|w\|_\Sigma = \sqrt{w \top \Sigma w}$, the error rate of the linear model writes $\text{err}(w) = \Phi(-\frac{a_w}{2})$ where $\Phi(x) = \frac{1}{\sqrt{2\pi}} \int_{-\infty}^x \exp(-\frac{t^2}{2}) dt$ is the cumulative distribution function of the standard normal distribution. Notice that a_w is invariant by rescaling of w . It measures the alignment with the best model w^* independently of the weight vector’s norm. We refer to a_w as the “expertise level” of our model f . Interestingly, a_w also appears in the calibration and refinement errors for this simple model.

Theorem 5.1. *For proper loss ℓ , the calibration and refinement errors of our model are*

$$\begin{aligned} \mathcal{K}_\ell(w) &= \mathbb{E} \left[d_\ell \left(\sigma \left(\|w\|_\Sigma \left(z + \frac{a_w}{2} \right) \right), \sigma \left(a_w \left(z + \frac{a_w}{2} \right) \right) \right) \right] \\ \mathcal{R}_\ell(w) &= \mathbb{E} \left[e_\ell \left(\sigma \left(a_w \left(z + \frac{a_w}{2} \right) \right) \right) \right], \end{aligned}$$

where the expectation is taken on $z \sim \mathcal{N}(0, 1)$.

Notice that the refinement error is a decreasing function of a_w , just like the error rate. Moreover, it depends on w via a_w only and so it is invariant by rescaling of the weight vector. In contrast, calibration error is not invariant by rescaling w . It is minimized, and reaches zero, when $\|w\|_\Sigma = a_w$. The larger the norm of the weight vector $\|w\|_\Sigma$, the larger the predicted probabilities $\sigma(w \top x)$, so $\|w\|_\Sigma$ can be interpreted as the model’s “confidence level.” The model is calibrated when this confidence level equals the expertise level a_w . A consequence is that there always exists a rescaling of the weight vector for which the calibration error cancels.

Theorem 5.2. *The re-scaled weight vector $w_s \leftarrow sw$ with $s = \langle w, w^* \rangle_\Sigma / \|w\|_\Sigma^2$ yields null calibration error $\mathcal{K}(w_s) = 0$ while preserving the refinement error $\mathcal{R}(w_s) = \mathcal{R}(w)$.*

Note that such rescaling of the weight vector exactly corresponds to temperature scaling. For classifiers like logistic regression or neural nets that use a sigmoid to produce probabilities, Theorem 5.2 establishes that, under the assumption that the logit distribution is a mixture of Gaussians, TS sets calibration error to zero while preserving refinement. To the best of our knowledge, this is the first theoretical guarantee for temperature scaling. An immediate corollary of this and Theorem 2.1 is that refinement error equals risk after temperature scaling: $\mathcal{R}(w) = \min_{s \in \mathbb{R}} \text{Risk}(sw)$.

Remark 5.3. For non-centered or imbalanced data, adding an intercept parameter to TS is necessary to achieve the same

result. A similar analysis can be derived for the multi-class case, leading to post-hoc calibration with matrix scaling.

This supports the idea that we should minimize refinement during training. Rescaling the weight vector to the correct confidence level is enough to remove the calibration error after training. From our analysis, it seems clear that calibration and refinement error minimizers do not have to match. The confidence level $\|w\|_\Sigma$ is not constrained to equal the expertise a_w in any way. We observed empirically that loss and refinement minimizers can be separated. Can we push the analysis further to exhibit this theoretically?

6. High dimensional asymptotics of logistic regression

In this section, we place ourselves in the setting of regularized logistic regression to study the impact of calibration and refinement on the risk during training. Proofs and missing technical details are provided in Appendix D.

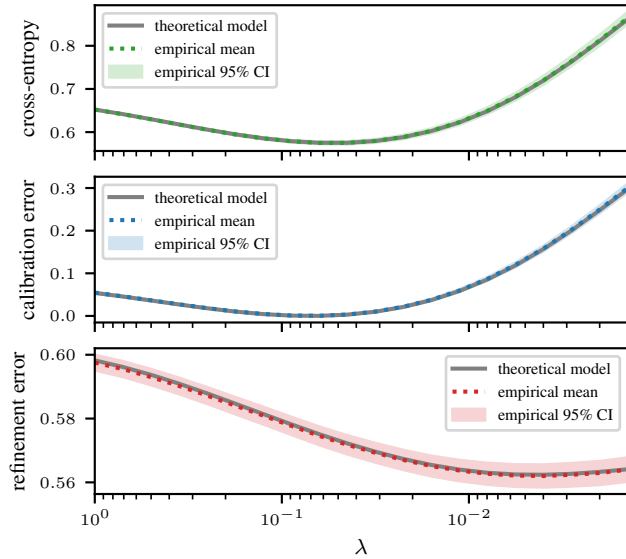


Figure 6: Cross-entropy, calibration and refinement errors when λ varies. The spectral distribution F is uniform ($\alpha = \beta = 1$), $e^* = 10\%$, and $r = \frac{1}{2}$. We fit a logistic regression on 2000 random samples from our data model to obtain \hat{w}_λ . We compute the resulting calibration and refinement errors using Theorem 5.1 and plot 95% error bars after 50 seeds. Theory closely matches empirical observations.

Consider n pairs $(x_i, y_i)_{1 \leq i \leq n}$ from the bimodal data model of Section 5 and w_λ the weight vector learned by solving regularized logistic regression

$$\min_{w \in \mathbb{R}^p} \frac{1}{n} \sum_{i=1}^n \log(1 + \exp(-y_i w^\top X_i)) + \frac{\lambda}{2} \|w\|^2,$$

for a given regularization strength $\lambda \in \mathbb{R}_+$.

We will exploit known results on w_λ in the high-dimensional asymptotic setting $n, p \rightarrow \infty$ with a constant ratio $p/n \rightarrow r > 0$. We assume that the class means on each dimension $(\mu_i)_{1 \leq i \leq p}$ are sampled i.i.d. from a distribution satisfying $\mathbb{E}[\mu_i^2] = \frac{c^2}{p}$, such that $\|\mu\|_2 \xrightarrow{p \rightarrow \infty} c$ for some constant $c > 0$ that controls the class separability of the problem. To simplify the formulas, we assume that Σ is diagonal. We further assume its eigenvalues $(\sigma_i)_{1 \leq i \leq p}$ are sampled i.i.d. from a positive, bounded spectral distribution F . Mai et al. (2019) provide the following characterization of w_λ

$$w_\lambda \sim \mathcal{N}\left(\eta(\lambda I_p + \tau \Sigma)^{-1} \mu, \frac{\gamma}{n} (\lambda I_p + \tau \Sigma)^{-1} \Sigma (\lambda I_p + \tau \Sigma)^{-1}\right),$$

where τ, η, γ are the unique solutions to a non-linear system of equations, parametrized by r, c, λ and F . To compute calibration and refinement errors that appear in Theorem 5.1, we are interested in $\langle w_\lambda, w^* \rangle_\Sigma$ and $\|w_\lambda\|_\Sigma$.

Proposition 6.1. For $n, p \rightarrow \infty$,

$$\langle w_\lambda, w^* \rangle_\Sigma \xrightarrow{P} \mathbb{E}_{\sigma \sim F} \left[\frac{2\eta c^2}{\lambda + \tau\sigma} \right],$$

$$\|w_\lambda\|_\Sigma^2 \xrightarrow{P} \mathbb{E}_{\sigma \sim F} \left[\frac{\gamma r \sigma^2 + \eta^2 c^2 \sigma}{(\lambda + \tau\sigma)^2} \right],$$

where the convergence is in probability.

Remark 6.2. Results from Dobriban & Wager (2018) allow to derive similar results for regularized LDA and Ridge, leading to simpler formulations of refinement and calibration errors. We omit these results for space constraints.

The data separability parameter c is hard to interpret; instead, we work with e^* , the error rate of the optimal classifier w^* .

Proposition 6.3. As $n, p \rightarrow \infty$,

$$e^* \xrightarrow{a.s.} \Phi\left(-c \sqrt{\mathbb{E}_{\sigma \sim F}[\sigma^{-1}]}\right).$$

e^* provides a common and interpretable scale for the problem difficulty, whatever the shape of the spectral distribution. Given a spectral distribution F , Proposition 6.3 gives a simple relation between e^* and c . We can choose any bounded and positive distribution F in our formulas to compute $\langle w_\lambda, w^* \rangle_\Sigma$ and $\|w_\lambda\|_\Sigma^2$. We pick $\sigma = \varepsilon + B(\alpha, \beta)$ where B denotes a Beta distribution with shape parameters (α, β) and ε is a small shift parameter to make F strictly positive (given that e^* is always finite, we fix $\varepsilon = 10^{-3}$). This allows us to explore a variety of spectral distribution shapes with a single mathematical model, by tweaking α and β . Using Propositions 6.1 and 6.3, we obtain formulas for $\langle w_\lambda, w^* \rangle_\Sigma$, $\|w_\lambda\|_\Sigma^2$ and e^* , see Appendix D.

For a given regularization strength λ , dimensions to samples ratio r , optimal error rate e^* and spectral distribution F (controlled by α, β), we can compute η, τ, γ by solving the system provided by Mai et al. (2019). Using Proposition 6.1

and Theorem 5.1 we obtain the calibration and refinement errors. We provide a fast implementation of this method at github.com/eugeneberta/RefineThenCalibrate-Theory. For a fixed set of parameters F, r, e^* , we can plot a learning curve for logistic regression by varying the amount of regularization λ . We observe the contributions of calibration and refinement errors to the total logloss of the model, as in Figure 6.

In this example, calibration and refinement errors are not minimized jointly, resulting in a loss minimizer somewhere between the two that is suboptimal for both errors. Given that we can easily set the calibration error to zero (Theorem 5.2), our mathematical model predicts that refinement-based early stopping yields a 2% decrease in downstream cross-entropy on this example.

We can explore the impact of problem parameters on this phenomenon. We investigate three spectral distribution shapes (first row). For each of these, we plot in Figure 7 the gap between the calibration error minimizer and the refinement error minimizer (second row) and the relative cross-entropy gains (%) obtained when stopping on refinement instead of loss (third row) as a function of the ratio $r = p/n$ (x-axis) and problem difficulty e^* (y-axis).

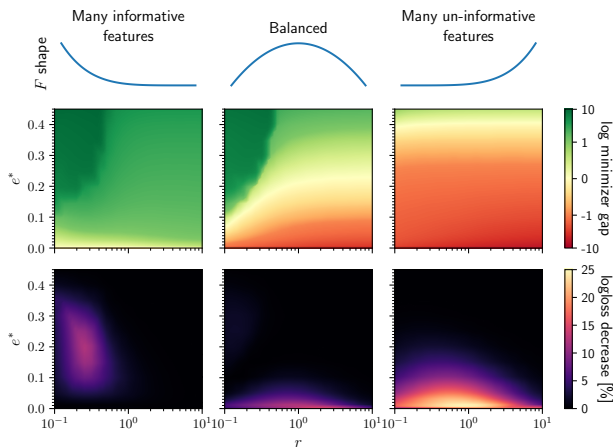


Figure 7: Influence of problem parameters on calibration and refinement minimizers. First row: spectral distribution shape. Second row: log gap between the two minimizers. In green regions, calibration is minimized earlier, while in red regions it is refinement. Third row: relative logloss gain (%) obtained with refinement-based early stopping.

To interpret spectral distribution shapes, note that a small eigenvalue translates to a small “within class variance” and thus more separable data on the corresponding axis. Smaller eigenvalues correspond to more informative features. The left column depicts a scenario where most features are equally informative. The central column has a wide spread

of good and bad features. In the right column, most features are bad while there are a few “hidden” good components. In the first scenario, calibration converges earlier almost everywhere on the parameter space, this corresponds to the regime we observe in computer vision. When informative features are scarce on the other hand, refinement is minimized earlier (right column). This might affect practical settings like genomics or histopathology. When the spectral distribution is more balanced, we see both scenarios co-existing, depending on problem parameters. Refinement-based early stopping always yields smaller loss, in the regions where the two minimizers are far apart (whichever error is minimized first), the gains are drastic with up to 25% loss decrease.

Remark 6.4. Bartlett et al. (2020) establish that benign overfitting occurs for linear regression in a similar data model under some condition on the spectral distribution of the covariance matrix. An avenue for future work is to study how this translates to classification and the link with the calibration-refinement decomposition.

7. Conclusion

We have demonstrated that selecting the best epoch and hyperparameters based on refinement error solves an issue that arises when using the validation loss. We established that refinement error can be estimated by the loss after post hoc calibration. This allowed us to use TS-refinement for early stopping, yielding improvement in test loss on various machine learning problems. Our estimator is available in the probmetrics package github.com/dholzmueller/probmetrics and can be used seamlessly with any architecture. One limitation is that TS-refinement can be more sensitive to overfitting on small validation sets. In this case, cross-validation, ensembling, and regularized post-hoc calibrators could be useful. Another little-explored area is the influence of training parameters—such as optimizers, schedulers, and regularization—on the calibration and refinement errors during training, raising the question of how refinement-based early stopping should be integrated with these parameters to maximize efficiency. While refinement-based stopping is relevant in data-constrained settings prone to overfitting, it could also prove useful for the fine-tuning of foundation models, where training long past the loss minimum can be beneficial (Ouyang et al., 2022; Carlsson et al., 2024). Additionally, while we explore its utility for model optimization, our refinement estimator could be a valuable diagnostic metric, especially in imbalanced multi-class settings where accuracy and area under the ROC curve are less appropriate.

Acknowledgements

The authors would like to thank Sacha Braun, Etienne Gauthier, Sebastian Gruber and Alexandre Perez-Lebel for fruitful discussions regarding this work.

This publication is part of the Chair “Markets and Learning”, supported by Air Liquide, BNP PARIBAS ASSET MANAGEMENT Europe, EDF, Orange and SNCF, sponsors of the Inria Foundation.

This work received support from the French government, managed by the National Research Agency, under the France 2030 program with the reference “PR[AI]RIE-PSAI” (ANR-23-IACL-0008).

Funded by the European Union (ERC-2022-SYG-OCEAN-101071601). Views and opinions expressed are however those of the author(s) only and do not necessarily reflect those of the European Union or the European Research Council Executive Agency. Neither the European Union nor the granting authority can be held responsible for them.

References

- Bach, F. High-dimensional analysis of double descent for linear regression with random projections. *SIAM Journal on Mathematics of Data Science*, 6(1):26–50, 2024.
- Bartlett, P. L., Long, P. M., Lugosi, G., and Tsigler, A. Benign overfitting in linear regression. *Proceedings of the National Academy of Sciences*, 117(48):30063–30070, 2020.
- Berta, E., Bach, F., and Jordan, M. Classifier calibration with ROC-regularized isotonic regression. In *Proceedings of The International Conference on Artificial Intelligence and Statistics*, 2024.
- Błasiok, J. and Nakkiran, P. Smooth ECE: Principled reliability diagrams via kernel smoothing. In *International Conference on Learning Representations*, 2024.
- Blasiok, J., Gopalan, P., Hu, L., and Nakkiran, P. When does optimizing a proper loss yield calibration? *Neural Information Processing Systems*, 36, 2024.
- Boyd, S. and Vandenberghe, L. *Convex Optimization*. Cambridge University Press, 2004.
- Brehmer, J. R. and Gneiting, T. Properization: constructing proper scoring rules via Bayes acts. *Annals of the Institute of Statistical Mathematics*, 72:659–673, 2020.
- Brier, G. W. Verification of forecasts expressed in terms of probability. *Monthly Weather Review*, 78(1):1–3, 1950.
- Bröcker, J. Reliability, sufficiency, and the decomposition of proper scores. *Quarterly Journal of the Royal Meteorological Society*, 135(643):1512–1519, 2009.
- Carlsson, F., Liu, F., Ward, D., Kurfali, M., and Nivre, J. The hyperfitting phenomenon: Sharpening and stabilizing llms for open-ended text generation. *arXiv:2412.04318*, 2024.
- Carrell, A. M., Mallinar, N., Lucas, J., and Nakkiran, P. The calibration generalization gap. *arXiv:2210.01964*, 2022.
- Chen, T. and Guestrin, C. XGBoost: A scalable tree boosting system. In *Proceedings of the International Conference on Knowledge Discovery and Data Mining*, pp. 785–794, 2016.
- Chidambaram, M. and Ge, R. Reassessing how to compare and improve the calibration of machine learning models. *arXiv:2406.04068*, 2024.
- Couillet, R., Liao, Z., and Mai, X. Classification asymptotics in the random matrix regime. In *European Signal Processing Conference*, pp. 1875–1879. IEEE, 2018.
- DeVries, T. Improved regularization of convolutional neural networks with cutout. *arXiv:1708.04552*, 2017.
- Dobriban, E. and Wager, S. High-dimensional asymptotics of prediction: Ridge regression and classification. *The Annals of Statistics*, 46(1):247–279, 2018.
- Erickson, N., Mueller, J., Shirkov, A., Zhang, H., Larroy, P., Li, M., and Smola, A. Autogluon-tabular: Robust and accurate automl for structured data. *arXiv:2003.06505*, 2020.
- Ferrer, L. and Ramos, D. Evaluating posterior probabilities: Decision theory, proper scoring rules, and calibration. *arXiv:2408.02841*, 2024.
- Fisher, R. A. The use of multiple measurements in taxonomic problems. *Annals of Eugenics*, 7(2):179–188, 1936.
- Gneiting, T. and Raftery, A. E. Strictly proper scoring rules, prediction, and estimation. *Journal of the American statistical Association*, 102(477):359–378, 2007.
- Gorishniy, Y., Rubachev, I., Khulkov, V., and Babenko, A. Revisiting deep learning models for tabular data. *Neural Information Processing Systems*, 34:18932–18943, 2021.
- Grinsztajn, L., Oyallon, E., and Varoquaux, G. Why do tree-based models still outperform deep learning on typical tabular data? *Neural Information Processing Systems*, 35: 507–520, 2022.
- Gruber, S. and Buettner, F. Better uncertainty calibration via proper scores for classification and beyond. *Neural Information Processing Systems*, 35:8618–8632, 2022.
- Gruber, S. G. and Bach, F. Optimizing estimators of squared calibration errors in classification. *arXiv:2410.07014*, 2024.

- Grünwald, P. D. and Dawid, A. P. Game theory, maximum entropy, minimum discrepancy and robust bayesian decision theory. *The Annals of Statistics*, 32(4):1367–1433, 2004.
- Guo, C., Pleiss, G., Sun, Y., and Weinberger, K. Q. On calibration of modern neural networks. In *International conference on machine learning*, 2017.
- He, K., Zhang, X., Ren, S., and Sun, J. Deep residual learning for image recognition. In *Proceedings of the Conference on Computer Vision and Pattern Recognition*, 2016.
- Holzmüller, D., Grinsztajn, L., and Steinwart, I. Better by default: Strong pre-tuned MLPs and boosted trees on tabular data. In *Neural Information Processing Systems*, 2024.
- Jordan, M. I. Why the logistic function? a tutorial discussion on probabilities and neural networks. *Computational Cognitive Science Technical Report 9503*, 1995.
- Kechris, A. S. *Classical Descriptive Set Theory*, volume 156 of *Graduate Texts in Mathematics*. Springer, 1995.
- Krizhevsky, A., Hinton, G., et al. Learning multiple layers of features from tiny images. 2009.
- Kull, M. and Flach, P. Novel decompositions of proper scoring rules for classification: Score adjustment as precursor to calibration. In *Machine Learning and Knowledge Discovery in Databases: European Conference*, 2015.
- Kull, M., Silva Filho, T., and Flach, P. Beta calibration: a well-founded and easily implemented improvement on logistic calibration for binary classifiers. In *Artificial Intelligence and Statistics*, pp. 623–631. PMLR, 2017.
- Kull, M., Perello Nieto, M., Kängsepp, M., Silva Filho, T., Song, H., and Flach, P. Beyond temperature scaling: Obtaining well-calibrated multi-class probabilities with dirichlet calibration. In *Advances in Neural Information Processing Systems*, 2019.
- Kumar, A., Liang, P. S., and Ma, T. Verified uncertainty calibration. In *Advances in Neural Information Processing Systems*, 2019.
- Liu, D. C. and Nocedal, J. On the limited memory bfgs method for large scale optimization. *Mathematical programming*, 45(1):503–528, 1989.
- Mai, X., Liao, Z., and Couillet, R. A large scale analysis of logistic regression: Asymptotic performance and new insights. In *International Conference on Acoustics, Speech and Signal Processing (ICASSP)*, 2019.
- Manokhin, V. Multi-class probabilistic classification using inductive and cross venn–abers predictors. In *Conformal and Probabilistic Prediction and Applications*, pp. 228–240. PMLR, 2017.
- McElfresh, D., Khandagale, S., Valverde, J., Prasad C, V., Ramakrishnan, G., Goldblum, M., and White, C. When do neural nets outperform boosted trees on tabular data? *Neural Information Processing Systems*, 36, 2024.
- Minderer, M., Djolonga, J., Romijnders, R., Hubis, F., Zhai, X., Houlsby, N., Tran, D., and Lucic, M. Revisiting the calibration of modern neural networks. *Neural Information Processing Systems*, 34:15682–15694, 2021.
- Murphy, A. H. A new vector partition of the probability score. *Journal of Applied Meteorology and Climatology*, 12(4):595–600, 1973.
- Naeini, M. P., Cooper, G., and Hauskrecht, M. Obtaining well calibrated probabilities using bayesian binning. In *Proceedings of the AAAI Conference on Artificial Intelligence*, 2015.
- Netzer, Y., Wang, T., Coates, A., Bissacco, A., Wu, B., Ng, A. Y., et al. Reading digits in natural images with unsupervised feature learning. In *NIPS workshop on deep learning and unsupervised feature learning*, volume 2011, pp. 4, 2011.
- Oron, A. P. and Flournoy, N. Centered isotonic regression: point and interval estimation for dose–response studies. *Statistics in Biopharmaceutical Research*, 9(3):258–267, 2017.
- Orseau, L. and Hutter, M. Line search for convex minimization. *arXiv:2307.16560*, 2023.
- Ouyang, L., Wu, J., Jiang, X., Almeida, D., Wainwright, C., Mishkin, P., Zhang, C., Agarwal, S., Slama, K., Ray, A., et al. Training language models to follow instructions with human feedback. *Neural Information Processing Systems*, 35:27730–27744, 2022.
- Pedregosa, F., Varoquaux, G., Gramfort, A., Michel, V., Thirion, B., Grisel, O., Blondel, M., Prettenhofer, P., Weiss, R., Dubourg, V., et al. Scikit-learn: Machine learning in python. *Journal of Machine Learning Research*, 12:2825–2830, 2011.
- Perez-Lebel, A., Le Morvan, M., and Varoquaux, G. Beyond calibration: estimating the grouping loss of modern neural networks. In *International Conference on Learning Representations*, 2023.
- Platt, J. et al. Probabilistic outputs for support vector machines and comparisons to regularized likelihood methods. *Advances in Large Margin Classifiers*, 10(3):61–74, 1999.

- Pohle, M.-O. The Murphy decomposition and the calibration-resolution principle: A new perspective on forecast evaluation. *arXiv:2005.01835*, 2020.
- Robertson, T., Wright, F., and Dykstra, R. *Order Restricted Statistical Inference*. Probability and Statistics Series. Wiley, 1988. ISBN 978-0-471-91787-8.
- Roelofs, R., Cain, N., Shlens, J., and Mozer, M. C. Mitigating bias in calibration error estimation. In *International Conference on Artificial Intelligence and Statistics*, 2022.
- Salehi, F., Abbasi, E., and Hassibi, B. The impact of regularization on high-dimensional logistic regression. *Advances in Neural Information Processing Systems*, 2019.
- Sanders, F. On subjective probability forecasting. *Journal of Applied Meteorology and Climatology*, 2(2):191–201, 1963.
- Silva Filho, T., Song, H., Perello-Nieto, M., Santos-Rodriguez, R., Kull, M., and Flach, P. Classifier calibration: a survey on how to assess and improve predicted class probabilities. *Machine Learning*, 112(9): 3211–3260, 2023.
- Tao, L., Zhu, Y., Guo, H., Dong, M., and Xu, C. A benchmark study on calibration. In *International Conference on Learning Representations*, 2024.
- Vaicenavicius, J., Widmann, D., Andersson, C., Lindsten, F., Roll, J., and Schön, T. Evaluating model calibration in classification. In *International Conference on Artificial Intelligence and Statistics*, 2019.
- Vovk, V., Petej, I., and Fedorova, V. Large-scale probabilistic predictors with and without guarantees of validity. *Neural Information Processing Systems*, 28, 2015.
- Wang, D.-B., Feng, L., and Zhang, M.-L. Rethinking calibration of deep neural networks: Do not be afraid of overconfidence. In *Advances in Neural Information Processing Systems*, 2021.
- Ye, H.-J., Liu, S.-Y., Cai, H.-R., Zhou, Q.-L., and Zhan, D.-C. A closer look at deep learning methods on tabular datasets. *arXiv:2407.00956*, 2024.
- Zadrozny, B. and Elkan, C. Transforming classifier scores into accurate multiclass probability estimates. In *Proceedings of the International Conference on Knowledge Discovery and Data Mining*, 2002.
- Zagoruyko, S. Wide residual networks. *arXiv:1605.07146*, 2016.

Appendices

Appendix Contents.

A	Related work	13
B	Calibration, Refinement, and Sharpness	13
C	Proofs for Section 5	17
D	Proofs for Section 6	19
E	Temperature scaling implementation and TS-refinement	22
F	Computer vision experiments	23
G	Tabular experiments	24
G.1	Dataset size dependency	24
G.2	Other stopping metrics	24
G.3	Effect on other metrics	24
G.4	Stopping times	24
G.5	Methods	24
G.6	Datasets	24

A. Related work

Proper scoring rules. Proper scoring rules have been used in meteorology to assess the quality of forecasts, see [Gneiting & Raftery \(2007\)](#) for an overview. They can also be motivated from a decision-theoretic point of view: The downstream loss for a decision-maker that chooses Bayes acts, i.e., actions that are optimal if the prediction is true, is a proper scoring rule ([Grünwald & Dawid, 2004](#)). This construction also allows to properize non-proper scoring rules ([Brehmer & Gneiting, 2020](#)).

Decompositions of proper scores. For the Brier score ([Brier, 1950](#)), the calibration-refinement decomposition was introduced by [Sanders \(1963\)](#) and the calibration-sharpness decomposition (see Appendix B) was introduced by [Murphy \(1973\)](#). [Bröcker \(2009\)](#) generalized these decompositions to other proper scoring rules. [Kull & Flach \(2015\)](#) rewrite these decompositions purely in terms of divergences between different random variables and introduce more terms like irreducible, epistemic, and grouping loss. [Pohle \(2020\)](#) also provides alternative formulations. However, none of these formulations is variational.

Calibration. [Guo et al. \(2017\)](#) observed that neural networks at their time were often miscalibrated and that logloss can overfit much earlier than accuracy, although the amount of miscalibration can depend on architectural and other details ([Minderer et al., 2021](#); [Tao et al., 2024](#)). Many post-hoc calibrations have been proposed to address this issue. Some methods are forms of logistic regression, as in Platt scaling ([Platt et al., 1999](#)), Temperature/Vector/Matrix scaling ([Guo et al., 2017](#)), Beta calibration ([Kull et al., 2017](#)), and Dirichlet calibration ([Kull et al., 2019](#)). Another family of methods stems from isotonic regression ([Robertson et al., 1988](#); [Zadrozny & Elkan, 2002](#); [Oron & Flournoy, 2017](#); [Vovk et al., 2015](#); [Manokhin, 2017](#); [Berta et al., 2024](#)). Approaches based on binning exist as well (e.g., [Naeini et al., 2015](#)) but are perhaps more popular for estimating calibration errors. [Wang et al. \(2021\)](#) demonstrate that changing the loss function can improve calibration before, but not after post-hoc calibration.

Post-hoc calibration and proper scores. [Gruber & Buettner \(2022\)](#) use a quantity similar to the loss for comparing post-hoc calibration methods, and [Gruber & Bach \(2024\)](#) propose a variational formulation for optimizing estimators of squared calibration errors. [Ferrer & Ramos \(2024\)](#) propose to look at the loss improvement through post-hoc recalibration as a measure of calibration error. The importance of optimizing the total loss and not only calibration error is emphasized, for example, by [Perez-Lebel et al. \(2023\)](#), [Chidambaram & Ge \(2024\)](#), and [Ferrer & Ramos \(2024\)](#). While we use a refinement estimator, [Perez-Lebel et al. \(2023\)](#) propose a grouping loss estimator that could be applicable in our case since the irreducible loss in our case is independent of f . However, the grouping loss is harder to estimate than the refinement loss since a grouping loss estimator can be used to estimate the irreducible loss $\inf_f \text{Risk}(f)$.

High dimensional asymptotics of classification. Our analysis of classification and refinement errors for regularized logistic regression in the high-dimensional setting builds upon a rich literature. More specifically [Dobriban & Wager \(2018\)](#); [Mai et al. \(2019\)](#) study classification error with the same data model and provide asymptotic results that are directly applicable in our analysis. [Couillet et al. \(2018\)](#); [Salehi et al. \(2019\)](#) study adjacent scenarios that we experimented with. [Bach \(2024\)](#) provides a new perspective on these high dimensional results through the lens of self-induced regularization, that could prove relevant to interpret the formulas obtained for calibration and refinement errors.

B. Calibration, Refinement, and Sharpness

In the following, we prove Theorem B.1, which is a more general version of Theorem 2.1. Figure B.1 illustrates the relation between terms in these decompositions. In particular, it includes the calibration-sharpness decomposition ([Bröcker, 2009](#)) given by

$$\text{Risk}(f) = \mathbb{E}[\ell(f(X), Y)] = e_\ell(\mathbb{E}[Y]) - \underbrace{\mathbb{E}[d_\ell(\mathbb{E}[Y], C)]}_{\text{Sharpness } \mathcal{S}_\ell(f)} + \underbrace{\mathbb{E}[d_\ell(f(X), C)]}_{\text{Calib. error } \mathcal{K}_\ell(f)}.$$

For the following results, we use a more technically precise definition of proper losses. We follow ([Gneiting & Raftery, 2007](#)) but reverse the sign such that proper losses should be minimized instead of maximized. We consider losses $\ell : \Delta_k \times \mathcal{Y}_k \rightarrow \mathbb{R} \cup \{\infty\}$ such that $\ell(P, \cdot)$ is Q -quasi-integrable for all $P, Q \in \Delta_k$. The latter condition is necessary such that $\ell(P, Q)$ is defined. The conditions could be further relaxed to use convex subsets of Δ_k , which we omit for simplicity.

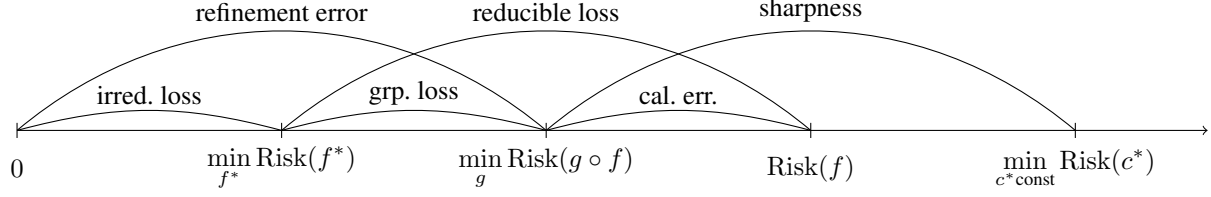


Figure B.1: Relation between different terms relating to proper scoring rules, proven in Theorem B.1. Here, infima are over measurable functions. A line $A \overset{u}{-} B$ means $u = B - A$. “irred.” stands for irreducible and “grp.” for grouping. For the definitions, see Remark B.2.

Theorem B.1 (Extended variational reformulations). *Let $k \geq 2$, let $\ell : \Delta_k \times \mathcal{Y}_k \rightarrow \mathbb{R} \cup \{\infty\}$ be a proper loss, and let $f : \mathcal{X} \rightarrow \Delta_k$ be measurable, where Δ_k is equipped with the Borel σ -algebra. Then,*

$$\begin{aligned} \mathcal{R}_\ell(f) &= \min_g \text{Risk}(g \circ f), \\ \mathcal{K}_\ell(f) &= \text{Risk}(f) - \min_g \text{Risk}(g \circ f), \\ \mathcal{S}_\ell(f) &= \min_{c \text{ constant}} \text{Risk}(c) - \min_g \text{Risk}(g \circ f), \\ e_\ell(\mathbb{E}[Y]) &= \min_{c \text{ constant}} \text{Risk}(c). \end{aligned}$$

Here, the minima are over measurable functions $g : \Delta_k \rightarrow \Delta_k$ and $c : \mathcal{X} \rightarrow \Delta_k$. They are attained by $g^*(q) := \mathbb{E}[Y|f(X) = q]$ and $c^*(x) := \mathbb{E}[Y]$. If ℓ is strictly proper, the minimizers are unique up to $P_{f(X)}$ -null sets.

Proof. Let $g_C(q) := \mathbb{E}[Y|f(X) = q]$, such that $C = \mathbb{E}[Y|f(X)] = g_C(f(X))$ almost surely. Then,

$$\begin{aligned} \mathcal{R}_\ell(f) &= \mathbb{E}[e_\ell(C)] = \mathbb{E}[\ell(C, C)] = \mathbb{E}[\ell(g_C(f(X)), \mathbb{E}[Y|f(X)])] && \text{(by definition)} \\ &= \mathbb{E}[\ell(g_C(f(X)), Y)] && \text{(by Lemma B.6)} \\ &= \min_g \mathbb{E}[\ell(g(f(X)), Y)]. && \text{(by Lemma B.7 with } Z = f(X)) \end{aligned}$$

This shows the representation of the refinement error, and Lemma B.7 also shows that g^* is a minimizer, which is almost surely unique. The representation of the calibration error follows directly from the calibration-refinement decomposition $\text{Risk}(f) = \mathcal{R}_\ell(f) + \mathcal{K}_\ell(f)$ (Bröcker, 2009).

Now, let $Z \in \Delta_k$ be the uniform distribution (to be interpreted as a constant random variable). Then, for $\bar{p} := \mathbb{E}[Y]$

$$\begin{aligned} e_\ell(\mathbb{E}[Y]) &= \ell(\mathbb{E}[Y], \mathbb{E}[Y]) = \ell(\bar{p}, \mathbb{E}[Y]) \\ &= \mathbb{E}[\ell(\bar{p}, Y)] && (\ell \text{ is affine in the second argument)} \\ &= \min_g \mathbb{E}[\ell(g(Z), Y)] && \text{(by Lemma B.7)} \\ &= \min_{c \text{ constant}} \mathbb{E}[\ell(c(f(X)), Y)]. \end{aligned}$$

Again, Lemma B.7 shows that the minimizer is $c^*(q) = \mathbb{E}[Y|Z] = \mathbb{E}[Y]$.

For the sharpness, we have

$$\mathcal{S}_\ell(f) = \mathbb{E}[d_\ell(\mathbb{E}[Y], C)] = \mathbb{E}[\ell(\mathbb{E}[Y], C)] - \mathbb{E}[\ell(C, C)] = \mathbb{E}[\ell(\mathbb{E}[Y], \mathbb{E}[Y|f(X)])] - \mathcal{R}_\ell(f)$$

by definition. We already showed above that $\mathcal{R}_\ell(f) = \min_g \text{Risk}(g \circ f)$. For the other term, we exploit that ℓ is affine in its second argument to obtain

$$\mathbb{E}[\ell(\mathbb{E}[Y], \mathbb{E}[Y|f(X)])] = \ell(\mathbb{E}[Y], \mathbb{E}[\mathbb{E}[Y|f(X)]]) = e_\ell(\mathbb{E}[Y]). \quad \square$$

Remark B.2 (Alternative decompositions by Kull & Flach (2015)). Kull & Flach (2015) provide a slightly different calibration-refinement decomposition:

$$\mathbb{E}[d_\ell(f(X), Y)] = \underbrace{\mathbb{E}[d_\ell(f(X), C)]}_{\mathcal{K}_\ell(f)} + \underbrace{\mathbb{E}[d_\ell(C, Y)]}_{=:\mathcal{R}_\ell(f)} .$$

The alternative refinement error

$$\tilde{\mathcal{R}}_\ell(f) = \mathbb{E}[d_\ell(C, Y)] = \mathbb{E}[\ell(C, Y)] - \mathbb{E}[\ell(Y, Y)] = \mathcal{R}_\ell(f) - \mathbb{E}[\ell(Y, Y)]$$

equals $\mathcal{R}_\ell(f)$ if $\mathbb{E}[\ell(Y, Y)] = 0$, which is the case for logloss and Brier loss. In this case, the irreducible and grouping loss in Figure B.1 also equal the definitions of Kull & Flach (2015) in their decomposition

$$\mathbb{E}[d_\ell(C, Y)] = \underbrace{\mathbb{E}[d_\ell(C, \mathbb{E}[Y|X])]}_{\text{grouping loss}} + \underbrace{\mathbb{E}[d_\ell(\mathbb{E}[Y|X], Y)]}_{\text{irreducible loss}} .$$

Intuitively, the grouping loss describes the loss that occurs when $f(x_1) = f(x_2)$ but $\mathbb{E}[Y|X = x_1] \neq \mathbb{E}[Y|X = x_2]$.

The reducible loss in Figure B.1 is called *epistemic loss* in Kull & Flach (2015).

Remark B.3 (Extending the definitions of calibration, refinement, and sharpness). Theorem 2.1 shows that for proper losses, calibration error is not only a divergence relative to a desired target (C), but also a potential reduction in loss through post-processing. The latter perspective has been suggested by Ferrer & Ramos (2024) without showing equivalence to the former perspective. On the one hand, an advantage of the former perspective is that it extends to non-divergences like the L^1 distance. On the other hand, an advantage of the latter perspective is that it can be used to extend the notion of calibration error, refinement error, and sharpness to non-proper losses (changing the desired target) or even non-probabilistic settings such as regression with MSE loss. Moreover, refinement error and sharpness can even be defined when $f(X)$ is not in the right space for the loss function, for example because it is a hidden-layer representation in a neural network. The variational formulation also allows to define more related quantities by using various function classes \mathcal{G} and considering

$$\inf_{g \in \mathcal{G}} \text{Risk}(g \circ f) .$$

For example, considering the corresponding variant of calibration error for 1-Lipschitz functions, we obtain the post-processing gap from Blasiok et al. (2024). In the binary case, using increasing functions, we obtain the best possible risk attainable by isotonic regression.

Theorem B.1 also implies some further properties of calibration, refinement, and sharpness:

Corollary B.4. Let $k \geq 2$, let $\ell : \Delta_k \times \mathcal{Y}_k \rightarrow \mathbb{R} \cup \{\infty\}$ be a proper loss, and let $f : \mathcal{X} \rightarrow \Delta_k$ be measurable, where Δ_k is equipped with the Borel σ -algebra.

- (a) If f is calibrated, then its population risk cannot be reduced by post-processing, i.e., $\text{Risk}(f) = \inf_g \text{Risk}(g \circ f)$. The converse holds if ℓ is strictly proper (Blasiok et al., 2024).
- (b) Let $g : \Delta_k \rightarrow \Delta_k$ be measurable. Then, $\mathcal{R}_\ell(g \circ f) \geq \mathcal{R}_\ell(f)$, and $\mathcal{S}_\ell(g \circ f) \leq \mathcal{S}_\ell(f)$.
- (c) Let $g : \Delta_k \rightarrow \Delta_k$ be measurable and injective. Then, $\mathcal{R}_\ell(g \circ f) = \mathcal{R}_\ell(f)$, and $\mathcal{S}_\ell(g \circ f) = \mathcal{S}(f)$. (A similar result has been shown in Proposition 4.5 of Gruber & Buettner (2022).)
- (d) Suppose f is injective with a measurable left inverse (see Theorem B.5 for a sufficient condition). Then, the grouping loss is zero, that is, $\mathcal{R}_\ell(f) = \inf_{\tilde{f}} \mathcal{R}_\ell(\tilde{f})$ and $\mathcal{S}_\ell(f) = \sup_{\tilde{f}} \mathcal{R}_\ell(\tilde{f})$.

Proof.

- (a) By definition, f is calibrated iff $f(X) = \mathbb{E}[Y|f(X)]$ almost surely. By Theorem B.1, $\text{Risk}(g \circ f)$ is minimized by $g^*(q) = \mathbb{E}[Y|f(X) = q] = q$, where the equality holds $P_{f(X)}$ -almost surely. Hence, $\text{Risk}(f) = \inf_g \text{Risk}(g \circ f)$. For the converse, by Theorem B.1, if ℓ is strictly proper, the minimizer of $\text{Risk}(g \circ f)$ is unique up to $P_{f(X)}$ -null sets, hence $\mathbb{E}[Y|f(X) = q] = g^*(q) = q$ for $P_{f(X)}$ -almost all q , hence $\mathbb{E}[Y|f(X)] = f(X)$ almost surely.
- (b) Since $h \circ g$ is measurable for all measurable h , we have

$$\mathcal{R}_\ell(g \circ f) = \inf_h \text{Risk}((h \circ g) \circ f) \geq \inf_h \text{Risk}(h \circ f) = \mathcal{R}_\ell(f) .$$

The sharpness inequality follows analogously.

(c) Let $h^* \in \operatorname{argmin}_h \operatorname{Risk}(h \circ f)$. By Theorem B.5, there exists a measurable left inverse g^{-1} of g . Then,

$$\mathcal{R}_\ell(g \circ f) \leq \operatorname{Risk}((h^* \circ g^{-1}) \circ (g \circ f)) = \operatorname{Risk}(h^* \circ f) = \mathcal{R}_\ell(f),$$

which, together with (b), yields the claim for the refinement. The argument for sharpness is analogous.

(d) This follows analogously to (c). □

Theorem B.5 (Existence of measurable left inverses). *Let $(X, \mathcal{B}_X), (Y, \mathcal{B}_Y)$ be complete separable metric spaces with their associated Borel σ -Algebra, and let $f : X \rightarrow Y$ be measurable and injective. Then, there exists $g : Y \rightarrow X$ measurable with $g \circ f = \operatorname{id}$.*

Proof. By Corollary 15.2 in (Kechris, 1995), f is a Borel isomorphism from X to $f(X)$, so its inverse $f^{-1} : f(X) \rightarrow X$ is measurable. But then, for a fixed $y_0 \in Y$,

$$g : Y \rightarrow X, y \mapsto \begin{cases} f^{-1}(y) & , y \in f(X) \\ y_0 & , y \notin f(X) \end{cases}$$

is a measurable left-inverse to f , proving the claim. □

Lemma B.6. *Let $(Z, Y) \in \mathcal{Z} \times \mathcal{Y}_k$ be random variables with distribution P and let ℓ be proper. Then,*

$$\mathbb{E}[\ell(g(Z), \mathbb{E}[Y|Z])] = \mathbb{E}[\ell(g(Z), Y)].$$

Proof. Since \mathcal{Y}_k is a Radon space, there exists a regular conditional probability distribution $P_{Y|Z}$, using which we obtain

$$\begin{aligned} \mathbb{E}[\ell(g(Z), \mathbb{E}[Y|Z])] &= \int \ell(g(z), \int y P_{Y|Z}(dy|z)) dP_Z(z) \\ &= \int \int \ell(g(z), y) P_{Y|Z}(dy|z) dP_Z(z) && \text{(since } \ell \text{ is affine in the second argument)} \\ &= \int \ell(g(z), y) dP(y, z) \\ &= \mathbb{E}[\ell(g(Z), Y)]. \end{aligned} \quad \square$$

The following lemma, used in the proof of Theorem B.1, provides a formal version of a well-known result.

Lemma B.7. *Let $(Z, Y) \in \mathcal{Z} \times \mathcal{Y}_k$ be random variables and let ℓ be proper. Then, for measurable $g : \mathcal{Z} \rightarrow \mathcal{Y}$,*

$$\operatorname{Risk}(g) := \mathbb{E}[\ell(g(Z), Y)]$$

is minimized by $g^(z) := \mathbb{E}[Y|Z = z]$. If ℓ is strictly proper, then g^* is the unique minimizer up to P_Z -null sets.*

Proof. We have

$$\begin{aligned} \mathbb{E}[\ell(g(Z), Y)] &= \mathbb{E}[\ell(g(Z), \mathbb{E}[Y|Z])] && \text{(by Lemma B.6)} \\ &\geq \mathbb{E}[\ell(\mathbb{E}[Y|Z], \mathbb{E}[Y|Z])] && (\ell \text{ is proper)} \\ &= \mathbb{E}[\ell(\mathbb{E}[Y|Z], Y)] && \text{(by Lemma B.6)} \\ &= \mathbb{E}[\ell(g^*(Z), Y)]. \end{aligned}$$

If $\operatorname{Risk}(g) = \operatorname{Risk}(g^*)$, the inequality above can only be strict for z in a P_Z -null set. If ℓ is strictly proper, then the inequality is violated whenever $g^*(z) \neq g(z)$. □

C. Proofs for Section 5

Under the data model introduced in Section 5, $\mathbb{P}(Y = 1|X = x) = \sigma(w^{\top}x)$ with $w^* = 2\Sigma^{-1}\mu$ and $\sigma(x) = \frac{1}{1+e^{-x}}$.

Proof.

$$\begin{aligned}
 \mathbb{P}(Y = 1|X = x) &= \frac{\mathbb{P}(X = x|Y = 1)\mathbb{P}(Y = 1)}{\mathbb{P}(X = x)} \quad \text{using Bayes' theorem.} \\
 &= \frac{\mathbb{P}(X = x|Y = 1)\mathbb{P}(Y = 1)}{\mathbb{P}(X = x|Y = 1)\mathbb{P}(Y = 1) + \mathbb{P}(X = x|Y = -1)\mathbb{P}(Y = -1)} \quad \text{using the law of total probability.} \\
 &= \frac{\mathcal{N}(x|\mu, \Sigma)}{\mathcal{N}(x|\mu, \Sigma) + \mathcal{N}(x|-\mu, \Sigma)} \quad \text{using that } \mathbb{P}(Y = 1) = \mathbb{P}(Y = -1) \text{ and our data model.} \\
 &= \sigma\left(\frac{1}{2}(x^{\top}\Sigma^{-1}\mu + \mu^{\top}\Sigma^{-1}x + x^{\top}\Sigma^{-1}\mu + \mu^{\top}\Sigma^{-1}x)\right) \quad \text{dividing up and down by } \mathcal{N}(x|\mu, \Sigma). \\
 &= \sigma(2\mu^{\top}\Sigma^{-1}x) = \sigma(w^{*\top}x)
 \end{aligned}$$

With $w^* = 2\Sigma^{-1}\mu$. □

We now prove the following lemmas that we will use to demonstrate Theorem 5.1.

Lemma C.1. $\mathbb{P}(Y = 1|f(X) = \sigma(z)) = \sigma\left(\frac{\langle w, w^* \rangle_{\Sigma}}{\|w\|_{\Sigma}^2} z\right)$.

Lemma C.2. $\mathbb{P}(f(X) = \sigma(z)) = \frac{1}{2}\mathcal{N}\left(z|\frac{\langle w, w^* \rangle_{\Sigma}}{2}, \|w\|_{\Sigma}^2\right) + \frac{1}{2}\mathcal{N}\left(z|-\frac{\langle w, w^* \rangle_{\Sigma}}{2}, \|w\|_{\Sigma}^2\right)$.

Proof.

$$\begin{aligned}
 \mathbb{P}(Y = 1|f(X) = \sigma(z)) &= \mathbb{P}(Y = 1|\sigma(w^{\top}X) = \sigma(z)) \\
 &= \mathbb{P}(Y = 1|w^{\top}X = z) \\
 &= \frac{\mathbb{P}(w^{\top}X = z|Y = 1)\mathbb{P}(Y = 1)}{\mathbb{P}(w^{\top}X = z)} \\
 &= \frac{\mathbb{P}(w^{\top}X = z|Y = 1)\mathbb{P}(Y = 1)}{\mathbb{P}(w^{\top}X = z|Y = 1)\mathbb{P}(Y = 1) + \mathbb{P}(w^{\top}X = z|Y = -1)\mathbb{P}(Y = -1)}
 \end{aligned}$$

Using that the affine transformation of a multivariate normal dist. is a normal dist. ($w^{\top}X \sim \mathcal{N}(\pm w^{\top}\mu, w^{\top}\Sigma w)$)

$$\begin{aligned}
 &= \frac{\mathcal{N}(z|w^{\top}\mu, w^{\top}\Sigma w)}{\mathcal{N}(z|w^{\top}\mu, w^{\top}\Sigma w) + \mathcal{N}(z|-w^{\top}\mu, w^{\top}\Sigma w)} \\
 &= \sigma\left(\frac{(z + w^{\top}\mu)^2 - (z - w^{\top}\mu)^2}{2w^{\top}\Sigma w}\right) = \sigma\left(\frac{2w^{\top}\mu}{w^{\top}\Sigma w} z\right) = \sigma\left(\frac{\langle w, w^* \rangle_{\Sigma}}{\|w\|_{\Sigma}^2} z\right)
 \end{aligned}$$

Along the way, we derived the distribution of $f(X)$:

$$\begin{aligned}
 \mathbb{P}(f(X) = \sigma(z)) &= \mathbb{P}(w^{\top}X = z|Y = 1)\mathbb{P}(Y = 1) + \mathbb{P}(w^{\top}X = z|Y = -1)\mathbb{P}(Y = -1) \\
 &= \frac{1}{2}\mathcal{N}(z|w^{\top}\mu, w^{\top}\Sigma w) + \frac{1}{2}\mathcal{N}(z|-w^{\top}\mu, w^{\top}\Sigma w) \\
 &= \frac{1}{2}\mathcal{N}\left(z|\frac{\langle w, w^* \rangle_{\Sigma}}{2}, \|w\|_{\Sigma}^2\right) + \frac{1}{2}\mathcal{N}\left(z|-\frac{\langle w, w^* \rangle_{\Sigma}}{2}, \|w\|_{\Sigma}^2\right)
 \end{aligned}$$

□

Theorem 5.1. For proper loss ℓ , the calibration and refinement errors of our model are

$$\begin{aligned}
 \mathcal{K}_{\ell}(w) &= \mathbb{E}\left[d_{\ell}\left(\sigma\left(\|w\|_{\Sigma}\left(z + \frac{a_w}{2}\right)\right), \sigma\left(a_w\left(z + \frac{a_w}{2}\right)\right)\right)\right] \\
 \mathcal{R}_{\ell}(w) &= \mathbb{E}\left[e_{\ell}\left(\sigma\left(a_w\left(z + \frac{a_w}{2}\right)\right)\right)\right],
 \end{aligned}$$

where the expectation is taken on $z \sim \mathcal{N}(0, 1)$.

Proof. The refinement error writes

$$\mathcal{R}(w) = \mathbb{E}_{f(X)}[e_\ell(\mathbb{E}[Y|f(X)])]$$

Using Lemma C.1 and Lemma C.2,

$$= \frac{1}{2} \int e_\ell \left(\sigma \left(\frac{\langle w, w^* \rangle_\Sigma}{\|w\|_\Sigma^2} z \right) \right) \mathcal{N} \left(z \mid \frac{\langle w, w^* \rangle_\Sigma}{2}, \|w\|_\Sigma^2 \right) dz + \frac{1}{2} \int e_\ell \left(\sigma \left(\frac{\langle w, w^* \rangle_\Sigma}{\|w\|_\Sigma^2} z \right) \right) \mathcal{N} \left(z \mid -\frac{\langle w, w^* \rangle_\Sigma}{2}, \|w\|_\Sigma^2 \right) dz$$

Taking $u = (z - \frac{\langle w, w^* \rangle_\Sigma}{2}) / \|w\|_\Sigma$ in the first integral and $u = (z + \frac{\langle w, w^* \rangle_\Sigma}{2}) / \|w\|_\Sigma$ in the second, we get

$$\mathcal{R}(w) = \frac{1}{2} \int e_\ell \left(\sigma \left(\frac{\langle w, w^* \rangle_\Sigma}{\|w\|_\Sigma} u + \frac{\langle w, w^* \rangle_\Sigma^2}{2\|w\|_\Sigma^2} \right) \right) \mathcal{N}(u|0, 1) du + \frac{1}{2} \int e_\ell \left(\sigma \left(\frac{\langle w, w^* \rangle_\Sigma}{\|w\|_\Sigma} u - \frac{\langle w, w^* \rangle_\Sigma^2}{2\|w\|_\Sigma^2} \right) \right) \mathcal{N}(u|0, 1) du$$

σ is anti-symmetric around zero, assuming e_ℓ symmetric around $\frac{1}{2}$ the two terms are equal, which simplifies the expression,

$$\mathcal{R}(w) = \mathbb{E}_{z \sim \mathcal{N}(0,1)} \left[e_\ell \left(\sigma \left(\frac{\langle w, w^* \rangle_\Sigma}{\|w\|_\Sigma} \left(z + \frac{\langle w, w^* \rangle_\Sigma}{2\|w\|_\Sigma} \right) \right) \right) \right].$$

Similarly for the calibration error

$$\begin{aligned} \mathcal{K}(w) &= \mathbb{E}_{f(X)}[d_\ell(f(X), \mathbb{E}[Y|f(X)])] \\ &= \frac{1}{2} \int d_\ell \left(\sigma(z), \sigma \left(\frac{\langle w, w^* \rangle_\Sigma}{\|w\|_\Sigma^2} z \right) \right) \mathcal{N} \left(z \mid \frac{\langle w, w^* \rangle_\Sigma}{2}, \|w\|_\Sigma^2 \right) dz \\ &\quad + \frac{1}{2} \int d_\ell \left(\sigma(z), \sigma \left(\frac{\langle w, w^* \rangle_\Sigma}{\|w\|_\Sigma^2} z \right) \right) \mathcal{N} \left(z \mid -\frac{\langle w, w^* \rangle_\Sigma}{2}, \|w\|_\Sigma^2 \right) dz \\ &= \frac{1}{2} \int d_\ell \left(\sigma \left(\|w\|_\Sigma z + \frac{\langle w, w^* \rangle_\Sigma}{2} \right), \sigma \left(\frac{\langle w, w^* \rangle_\Sigma}{\|w\|_\Sigma} z + \frac{\langle w, w^* \rangle_\Sigma^2}{2\|w\|_\Sigma^2} \right) \right) \mathcal{N}(z|0, 1) dz \\ &\quad + \frac{1}{2} \int d_\ell \left(\sigma \left(\|w\|_\Sigma z - \frac{\langle w, w^* \rangle_\Sigma}{2} \right), \sigma \left(\frac{\langle w, w^* \rangle_\Sigma}{\|w\|_\Sigma} z - \frac{\langle w, w^* \rangle_\Sigma^2}{2\|w\|_\Sigma^2} \right) \right) \mathcal{N}(z|0, 1) dz \end{aligned}$$

σ is anti-symmetric around zero, assuming d_ℓ symmetric around $\frac{1}{2}$ the two terms are equal,

$$\mathcal{K}(w) = \mathbb{E}_{z \sim \mathcal{N}(0,1)} \left[d_\ell \left(\sigma \left(\|w\|_\Sigma \left(z + \frac{\langle w, w^* \rangle_\Sigma}{2\|w\|_\Sigma} \right) \right), \sigma \left(\frac{\langle w, w^* \rangle_\Sigma}{\|w\|_\Sigma} \left(z + \frac{\langle w, w^* \rangle_\Sigma}{2\|w\|_\Sigma} \right) \right) \right) \right].$$

□

Theorem 5.2. *The re-scaled weight vector $w_s \leftarrow sw$ with $s = \langle w, w^* \rangle_\Sigma / \|w\|_\Sigma^2$ yields null calibration error $\mathcal{K}(w_s) = 0$ while preserving the refinement error $\mathcal{R}(w_s) = \mathcal{R}(w)$.*

Proof. $a_w = \frac{\langle w, w^* \rangle_\Sigma}{\|w\|_\Sigma}$ is invariant by rescaling. Given $s \in \mathbb{R}$, $w_s = sw$, we have that $a_{w_s} = \frac{\langle sw, w^* \rangle_\Sigma}{\|sw\|_\Sigma} = \frac{s \langle w, w^* \rangle_\Sigma}{s \|w\|_\Sigma} = a_w$. The expression of refinement error in Theorem 5.1 depends on w only via a_w so the refinement is invariant by rescaling.

The calibration error writes:

$$\mathcal{K}(w) = \mathbb{E}_{z \sim \mathcal{N}(0,1)} \left[d_\ell \left(\sigma \left(\|w\|_\Sigma \left(z + \frac{a_w}{2} \right) \right), \sigma \left(a_w \left(z + \frac{a_w}{2} \right) \right) \right) \right]$$

Since a_w is invariant by rescaling, taking $w_s = \frac{\langle w, w^* \rangle_\Sigma}{\|w\|_\Sigma^2} w$ yields

$$\begin{aligned} \mathcal{K}(w_s) &= \mathbb{E}_{z \sim \mathcal{N}(0,1)} \left[d_\ell \left(\sigma \left(\frac{\langle w, w^* \rangle_\Sigma}{\|w\|_\Sigma^2} \|w\|_\Sigma \left(z + \frac{a_w}{2} \right) \right), \sigma \left(a_w \left(z + \frac{a_w}{2} \right) \right) \right) \right] \\ &= \mathbb{E}_{z \sim \mathcal{N}(0,1)} \left[d_\ell \left(\sigma \left(a_w \left(z + \frac{a_w}{2} \right) \right), \sigma \left(a_w \left(z + \frac{a_w}{2} \right) \right) \right) \right] \\ &= 0 \quad \text{since } \ell \text{ is a proper score } (d_\ell(p, p) = 0). \end{aligned}$$

□

D. Proofs for Section 6

For this section, we rely heavily on the following result by [Mai et al. \(2019\)](#), on the limit distribution of the weight vector for regularized logistic regression, with regularization strength λ , when $n, p \rightarrow \infty$ with a fixed ratio $p/n \rightarrow r$:

$$w_\lambda \sim \mathcal{N}\left(\eta(\lambda I_p + \tau \Sigma)^{-1} \mu, \frac{\gamma}{n} (\lambda I_p + \tau \Sigma)^{-1} \Sigma (\lambda I_p + \tau \Sigma)^{-1}\right).$$

Proposition 6.1. For $n, p \rightarrow \infty$,

$$\begin{aligned} \langle w_\lambda, w^* \rangle_\Sigma &\xrightarrow{P} \mathbb{E}_{\sigma \sim F} \left[\frac{2\eta c^2}{\lambda + \tau \sigma} \right], \\ \|w_\lambda\|_\Sigma^2 &\xrightarrow{P} \mathbb{E}_{\sigma \sim F} \left[\frac{\gamma r \sigma^2 + \eta^2 c^2 \sigma}{(\lambda + \tau \sigma)^2} \right], \end{aligned}$$

where the convergence is in probability.

Proof. $\langle w_\lambda, w^* \rangle_\Sigma$ follows a normal distribution with mean $2\eta \mu^\top (\lambda I_p + \tau \Sigma)^{-1} \mu$ and variance $\frac{4\gamma}{n} \mu^\top (\lambda I_p + \tau \Sigma)^{-1} \Sigma (\lambda I_p + \tau \Sigma)^{-1} \mu$. Looking at the variance first:

$$\mathbb{V}(\langle w_\lambda, w^* \rangle_\Sigma) = \frac{4\gamma}{n} \sum_{i=1}^p \frac{\sigma_i \mu_i^2}{(\lambda + \tau \sigma_i)^2}$$

Using independence between μ_i and σ_i and the strong law of large numbers

$$\begin{aligned} \mathbb{V}(\langle w_\lambda, w^* \rangle_\Sigma) &\xrightarrow{p \rightarrow \infty} \frac{4\gamma}{n} p \mathbb{E}[\mu_i^2] \mathbb{E}\left[\frac{\sigma_i}{(\lambda + \tau \sigma_i)^2}\right] \\ &= \frac{4\gamma c^2}{n} \mathbb{E}\left[\frac{\sigma_i}{(\lambda + \tau \sigma_i)^2}\right] \xrightarrow{n \rightarrow \infty} 0 \end{aligned}$$

So $\langle w_\lambda, w^* \rangle_\Sigma$ concentrates on its mean:

$$\mathbb{E}(\langle w_\lambda, w^* \rangle_\Sigma) = 2\eta \sum_{i=1}^p \frac{\mu_i^2}{\lambda + \tau \sigma_i} \xrightarrow{p \rightarrow \infty} 2\eta p \mathbb{E}[\mu_i^2] \mathbb{E}\left[\frac{1}{\lambda + \tau \sigma_i}\right] = 2\eta c^2 \mathbb{E}\left[\frac{1}{\lambda + \tau \sigma_i}\right]$$

Studying $w_\lambda^\top \Sigma w_\lambda$ requires a bit more work. Denoting $\varepsilon = \mathcal{N}(0, 1)$,

$$\begin{aligned} w_\lambda^\top \Sigma w_\lambda &\sim \sum_{i=1}^p \sigma_i w_{\lambda i}^2 \\ &= \sum_{i=1}^p \sigma_i \left(\frac{\eta \mu_i}{\lambda + \tau \sigma_i} + \varepsilon \sqrt{\frac{\gamma \sigma_i}{n(\lambda + \tau \sigma_i)^2}} \right)^2 \\ &= \sum_{i=1}^p \frac{\eta^2 \mu_i^2 \sigma_i}{(\lambda + \tau \sigma_i)^2} + \sum_{i=1}^p \frac{2\eta \mu_i \sqrt{\gamma} \sigma_i^{3/2}}{\sqrt{n}(\lambda + \tau \sigma_i)^2} \varepsilon + \sum_{i=1}^p \frac{\gamma \sigma_i^2}{n(\lambda + \tau \sigma_i)^2} \varepsilon^2 \\ &\xrightarrow{p \rightarrow \infty} p \eta^2 \frac{c^2}{p} \mathbb{E}\left[\frac{\sigma}{(\lambda + \tau \sigma)^2}\right] + 0 + p \frac{\gamma}{n} \mathbb{E}\left[\frac{\sigma^2}{(\lambda + \tau \sigma)^2}\right] \\ &= \eta^2 c^2 \mathbb{E}\left[\frac{\sigma}{(\lambda + \tau \sigma)^2}\right] + \gamma r \mathbb{E}\left[\frac{\sigma^2}{(\lambda + \tau \sigma)^2}\right] \end{aligned}$$

□

Proposition 6.3. As $n, p \rightarrow \infty$,

$$e^* \xrightarrow{a.s.} \Phi\left(-c \sqrt{\mathbb{E}_{\sigma \sim F}[\sigma^{-1}]}\right).$$

Proof.

$$\text{err}(w^*) = \Phi\left(-\frac{\langle w^*, w^* \rangle_\Sigma}{2\|w^*\|_\Sigma}\right) = \Phi\left(-\frac{\sqrt{w^{*\top}\Sigma w^*}}{2}\right) = \Phi\left(-\sqrt{\mu^\top\Sigma^{-1}\mu}\right) \xrightarrow{a.s.} \Phi\left(-\sqrt{p\mathbb{E}[\mu^2]\mathbb{E}\left[\frac{1}{\sigma}\right]}\right) = \Phi\left(-c\sqrt{\mathbb{E}[\sigma^{-1}]}\right)$$

□

Deriving formulas for $\text{err}(w^*)$, $\langle w_\lambda, w^* \rangle_\Sigma$ and $\|w_\lambda\|_\Sigma$

$$\begin{aligned}\mathbb{E}[\sigma^{-1}] &= \int_0^1 \frac{1}{u+\varepsilon} \frac{u^{\alpha-1}(1-u)^{\beta-1}}{B(\alpha, \beta)} du \\ &= \frac{1}{\varepsilon B(\alpha, \beta)} \int_0^1 \left(1 + \frac{u}{\varepsilon}\right)^{-1} u^{\alpha-1} (1-u)^{\beta-1} du \\ &= \frac{{}_2F_1\left(1, \alpha, \alpha + \beta, -\frac{1}{\varepsilon}\right)}{\varepsilon}\end{aligned}$$

Altogether

$$\text{err}(w^*) = \Phi\left(-c\sqrt{\frac{1}{\varepsilon}{}_2F_1\left(1, \alpha, \alpha + \beta, -\frac{1}{\varepsilon}\right)}\right)$$

Lemma D.1. Denoting ${}_2F_1$ the hyper-geometric function, \mathcal{B} the Beta distribution and B the beta function,

$$\begin{aligned}\mathbb{E}_{u \sim \mathcal{B}(\alpha, \beta)} \left[\frac{1}{\lambda + \tau(\varepsilon + u)} \right] &= \int_0^1 \frac{1}{\lambda + \tau(\varepsilon + u)} \frac{u^{\alpha-1}(1-u)^{\beta-1}}{B(\alpha, \beta)} du \\ &= \frac{1}{(\lambda + \tau\varepsilon)B(\alpha, \beta)} \int_0^1 \left(1 + \frac{\tau}{\lambda + \tau\varepsilon}u\right)^{-1} u^{\alpha-1} (1-u)^{\beta-1} du \\ &= \frac{{}_2F_1\left(1, \alpha, \alpha + \beta, -\left(\frac{\lambda}{\tau} + \varepsilon\right)^{-1}\right)}{\lambda + \tau\varepsilon}\end{aligned}$$

$$\begin{aligned}\mathbb{E}_{u \sim \mathcal{B}(\alpha, \beta)} \left[\frac{1}{(\lambda + \tau(\varepsilon + u))^2} \right] &= \int_0^1 \frac{1}{(\lambda + \tau(\varepsilon + u))^2} \frac{u^{\alpha-1}(1-u)^{\beta-1}}{B(\alpha, \beta)} du \\ &= \frac{1}{(\lambda + \tau\varepsilon)^2 B(\alpha, \beta)} \int_0^1 \left(1 + \frac{\tau}{\lambda + \tau\varepsilon}u\right)^{-2} u^{\alpha-1} (1-u)^{\beta-1} du \\ &= \frac{{}_2F_1\left(2, \alpha, \alpha + \beta, -\left(\frac{\lambda}{\tau} + \varepsilon\right)^{-1}\right)}{(\lambda + \tau\varepsilon)^2}\end{aligned}$$

$$\begin{aligned}\mathbb{E}_{u \sim \mathcal{B}(\alpha, \beta)} \left[\frac{u}{(\lambda + \tau(\varepsilon + u))^2} \right] &= \int_0^1 \frac{u}{(\lambda + \tau(\varepsilon + u))^2} \frac{u^{\alpha-1}(1-u)^{\beta-1}}{B(\alpha, \beta)} du \\ &= \frac{1}{(\lambda + \tau\varepsilon)^2 B(\alpha, \beta)} \int_0^1 \left(1 + \frac{\tau}{\lambda + \tau\varepsilon}u\right)^{-2} u^\alpha (1-u)^{\beta-1} du \\ &= \frac{B(\alpha + 1, \beta)}{B(\alpha, \beta)(\lambda + \tau\varepsilon)^2} {}_2F_1\left(2, \alpha + 1, \alpha + \beta + 1, -\left(\frac{\lambda}{\tau} + \varepsilon\right)^{-1}\right)\end{aligned}$$

$$\begin{aligned}\mathbb{E}_{u \sim \mathcal{B}(\alpha, \beta)} \left[\frac{u^2}{(\lambda + \tau(\varepsilon + u))^2} \right] &= \int_0^1 \frac{u^2}{(\lambda + \tau(\varepsilon + u))^2} \frac{u^{\alpha-1}(1-u)^{\beta-1}}{B(\alpha, \beta)} du \\ &= \frac{1}{(\lambda + \tau\varepsilon)^2 B(\alpha, \beta)} \int_0^1 \left(1 + \frac{\tau}{\lambda + \tau\varepsilon}u\right)^{-2} u^{\alpha+1} (1-u)^{\beta-1} du \\ &= \frac{B(\alpha + 2, \beta)}{B(\alpha, \beta)(\lambda + \tau\varepsilon)^2} {}_2F_1\left(2, \alpha + 2, \alpha + \beta + 2, -\left(\frac{\lambda}{\tau} + \varepsilon\right)^{-1}\right)\end{aligned}$$

Using the equations in Lemma D.1 and the linearity of the expectation we get that

$$\langle w_\lambda, w^* \rangle_\Sigma \xrightarrow{(n,p) \rightarrow \infty} 2\eta c^2 \mathbb{E} \left[\frac{1}{\lambda + \tau\sigma} \right] = 2\eta c^2 \frac{{}_2F_1(1, \alpha, \alpha + \beta, -(\frac{\lambda}{\tau} + \varepsilon)^{-1})}{\lambda + \tau\varepsilon}.$$

Similarly,

$$\begin{aligned} \|w_\lambda\|_\Sigma^2 &\xrightarrow{(n,p) \rightarrow \infty} \eta^2 c^2 \mathbb{E} \left[\frac{\sigma}{(\lambda + \tau\sigma)^2} \right] + \gamma r \mathbb{E} \left[\frac{\sigma^2}{(\lambda + \tau\sigma)^2} \right] \\ &= \frac{\eta^2 c^2}{(\lambda + \tau\varepsilon)^2} \left(\varepsilon {}_2F_1(2, \alpha, \alpha + \beta, -(\frac{\lambda}{\tau} + \varepsilon)^{-1}) + \frac{B(\alpha + 1, \beta)}{B(\alpha, \beta)} {}_2F_1(2, \alpha + 1, \alpha + \beta + 1, -(\frac{\lambda}{\tau} + \varepsilon)^{-1}) \right) \\ &+ \frac{\gamma r}{(\lambda + \tau\varepsilon)^2} \left(\frac{B(\alpha + 2, \beta)}{B(\alpha, \beta)} {}_2F_1(2, \alpha + 2, \alpha + \beta + 2, -(\frac{\lambda}{\tau} + \varepsilon)^{-1}) + 2\varepsilon \frac{B(\alpha + 1, \beta)}{B(\alpha, \beta)} {}_2F_1(2, \alpha + 1, \alpha + \beta + 1, -(\frac{\lambda}{\tau} + \varepsilon)^{-1}) \right. \\ &\left. + \varepsilon^2 {}_2F_1(2, \alpha, \alpha + \beta, -(\frac{\lambda}{\tau} + \varepsilon)^{-1}) \right). \end{aligned}$$

Solving the non-linear system in (Mai et al., 2019) also requires computing κ :

$$\begin{aligned} \kappa &\xrightarrow{(n,p) \rightarrow \infty} r \mathbb{E} \left[\frac{\sigma}{\lambda - e\sigma} \right] \\ &= r \mathbb{E}_{u \sim \mathcal{B}(\alpha, \beta)} \left[\frac{u + \varepsilon}{\lambda - e(\varepsilon + u)} \right] \\ &= r \left(\int_0^1 \frac{u}{\lambda - e(\varepsilon + u)} \frac{u^{\alpha-1}(1-u)^{\beta-1}}{B(\alpha, \beta)} du + \varepsilon \int_0^1 \frac{1}{\lambda - e(\varepsilon + u)} \frac{u^{\alpha-1}(1-u)^{\beta-1}}{B(\alpha, \beta)} du \right) \\ &= \frac{r}{B(\alpha, \beta)(\lambda - e\varepsilon)} \left(\int_0^1 \left(1 - \frac{e}{\lambda - e\varepsilon} u\right)^{-1} u^\alpha (1-u)^{\beta-1} du + \varepsilon \int_0^1 \left(1 - \frac{e}{\lambda - e\varepsilon} u\right)^{-1} u^{\alpha-1} (1-u)^{\beta-1} du \right) \\ &= \frac{r}{\lambda - e\varepsilon} \left(\frac{B(\alpha + 1, \beta)}{B(\alpha, \beta)} {}_2F_1(1, \alpha + 1, \alpha + \beta + 1, (\frac{\lambda}{e} - \varepsilon)^{-1}) + \varepsilon \cdot {}_2F_1(1, \alpha, \alpha + \beta, (\frac{\lambda}{e} - \varepsilon)^{-1}) \right). \end{aligned}$$

We provide an efficient implementation of the non-linear system solver with our particular data model and functions to compute the resulting calibration and refinement errors at github.com/eugeneberta/RefineThenCalibrate-Theory.

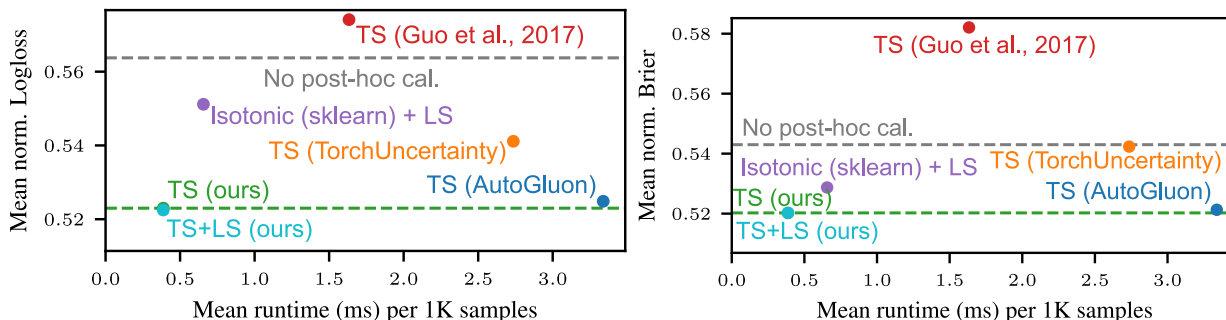


Figure E.1: **Runtime vs. mean benchmark scores of different TS implementations and isotonic regression for logloss (left) and Brier loss (right).** Runtimes are averaged over validation sets with at least 10K samples. The evaluation is on XGBoost models trained with default parameters, using the epoch with the best validation accuracy. The y -axis shows the mean of normalized logloss (left) or Brier loss (right), where normalizing means dividing by the loss $e_\ell(\mathbb{E}[Y])$ of the best constant predictor on each dataset.

E. Temperature scaling implementation and TS-refinement

For the logloss, the objective $\mathcal{L}(\beta) = \sum_{(x,y) \in \mathcal{D}} -y^\top \log(\text{softmax}(\beta \log(f(x))))$ is convex, which follows from the fact that $-\log(\text{softmax}(x)) = \text{logsumexp}(x) - x$ is convex (Boyd & Vandenberghe, 2004). Specifically, we use 30 bisection steps to approximate $b^* := \text{argmin}_{b \in [-16, 16]} \mathcal{L}(\exp(b))$ and then find $\beta^* := \exp(b^*)$. If even faster implementations are desired, more advanced line search for convex functions (Orseau & Hutter, 2023), second-order methods, stochastic optimization, or warm-starting could be helpful. To guard against overfitting in cases with 100% validation accuracy, where bisection can efficiently approach $\beta^* = \infty$, we introduce a form of Laplace smoothing (LS) as $g(p) := \frac{N_{\text{cal}}}{N_{\text{cal}}+1} g_{\beta^*}(p) + \frac{1}{N_{\text{cal}}+1} u$, where u is the uniform distribution and N_{cal} is the number of samples in the calibration set. This version is used for our main experiments except for Figure 3.

Extended comparison. Figure E.1 shows a comparison of more post-hoc calibration methods. While Figure 3 uses mean logloss for simplicity, this can over-emphasize multi-class datasets while imbalanced datasets get less weight. To compensate for this, in Figure E.1 we divide the loss (logloss or Brier loss) for each dataset by the loss of the best constant predictor, which can be written as $e_\ell(\mathbb{E}[Y])$.

Our inclusion of Laplace smoothing (LS) to TS brings a small benefit for logloss. We also compare our results to isotonic regression, where we include LS to avoid infinite logloss since IR can predict a probability of zero.¹ While the IR implementation from scikit-learn (Pedregosa et al., 2011) is almost as fast as our TS implementation, it performs considerably worse on our benchmark. For Brier loss, the benefit of TS in general is less pronounced, and only good implementations improve results compared to no post-hoc calibration.

Validation. We are interested in minimizing the population risk of calibrated estimators. To faithfully estimate the population risk, it is possible to use cross-validation or the holdout method, fitting the calibrator on a part of the validation set while using its loss on the remaining part as a refinement estimate. However, we experimentally observe in Figure G.2 that fitting and evaluating temperature scaling on the entire validation set works equally well, perhaps because it only fits a single parameter. We use the latter approach in the following since it is more efficient compared to cross-validation.

¹IVAP (Vovk et al., 2015) is a variant of isotonic regression that does not predict zero probabilities but we found it to be roughly two orders of magnitude slower than isotonic regression, so we did not consider it very attractive as a component of a refinement estimator.

F. Computer vision experiments

We train a ResNet-18 (He et al., 2016) and WideResNet (Zagoruyko, 2016) on CIFAR-10, CIFAR-100 and SVHN datasets (Krizhevsky et al., 2009; Netzer et al., 2011). We train for 300 epochs using SGD with momentum = 0.9, weight decay = 10^{-4} and a learning rate scheduler that divides the learning rate by ten every 100 epochs. We use random cropping (32×32 crops after padding images by 4 pixels), horizontal flips (pytorch default) and cutout (DeVries, 2017) (one 16×16 hole per image during training). We train each model ten times on each dataset. 10% of the training set is kept for validation. We select the best epoch based on different metrics evaluated on the validation set: logloss, Brier score, accuracy and logloss after temperature scaling (TS-refinement). On Table F.1 (ResNet-18) and Table F.2 (WideResNet) we report average logloss, brier score, accuracy, ECE and smooth ECE (Błasiok & Nakkiran, 2024) obtained for each stopping metric. Figure 1 is generated with the same training recipe with a cosine annealing scheduler instead to avoid big jumps in the loss landscape and no weight decay to exacerbate the effect of calibration overfitting. See github.com/eugeneberta/RefineThenCalibrate-Vision.

Dataset	Stopping metric	Logloss	Brier	Accuracy	ECE	smECE
CIFAR-10	Logloss	0.161 \pm 0.004	0.080 \pm 0.002	94.6% \pm 0.2	0.006 \pm 0.001	0.008 \pm 0.001
	Brier score	0.154 \pm 0.005	0.073 \pm 0.003	95.1% \pm 0.2	0.007 \pm 0.001	0.008 \pm 0.001
	Accuracy	0.155 \pm 0.005	0.074 \pm 0.003	95.1% \pm 0.2	0.007 \pm 0.001	0.009 \pm 0.001
	TS-refinement	0.154 \pm 0.005	0.074 \pm 0.003	95.1% \pm 0.2	0.007 \pm 0.002	0.008 \pm 0.001
CIFAR-100	Logloss	1.015 \pm 0.008	0.367 \pm 0.003	73.2% \pm 0.3	0.019 \pm 0.002	0.019 \pm 0.001
	Brier score	1.014 \pm 0.007	0.367 \pm 0.002	73.1% \pm 0.3	0.020 \pm 0.002	0.019 \pm 0.001
	Accuracy	1.001 \pm 0.012	0.366 \pm 0.003	73.1% \pm 0.3	0.018 \pm 0.001	0.018 \pm 0.001
	TS-refinement	0.983 \pm 0.008	0.366 \pm 0.003	73.0% \pm 0.2	0.016 \pm 0.001	0.016 \pm 0.001
SVHN	Logloss	0.120 \pm 0.003	0.048 \pm 0.001	96.9% \pm 0.1	0.006 \pm 0.001	0.007 \pm 0.001
	Brier score	0.118 \pm 0.002	0.048 \pm 0.001	97.0% \pm 0.1	0.006 \pm 0.001	0.007 \pm 0.001
	Accuracy	0.124 \pm 0.005	0.049 \pm 0.002	96.9% \pm 0.1	0.006 \pm 0.001	0.008 \pm 0.001
	TS-refinement	0.119 \pm 0.002	0.048 \pm 0.001	97.0% \pm 0.1	0.006 \pm 0.001	0.007 \pm 0.001

Table F.1: Benchmark results for ResNet-18. We plot means obtained over the 10 runs and 95% confidence intervals computed using the t-distribution. Stopping metrics are evaluated on the validation set (10% of training data). All metrics are reported for the best model as selected by the corresponding stopping metric, after TS (fitted using the validation set).

Dataset	Stopping metric	Logloss	Brier	Accuracy	ECE	smECE
CIFAR-10	Logloss	0.123 \pm 0.004	0.061 \pm 0.002	95.9% \pm 0.2	0.006 \pm 0.001	0.008 \pm 0.000
	Brier score	0.121 \pm 0.002	0.056 \pm 0.001	96.4% \pm 0.1	0.006 \pm 0.001	0.008 \pm 0.001
	Accuracy	0.122 \pm 0.002	0.056 \pm 0.001	96.4% \pm 0.1	0.006 \pm 0.001	0.008 \pm 0.001
	TS-refinement	0.120 \pm 0.002	0.056 \pm 0.001	96.3% \pm 0.1	0.007 \pm 0.001	0.008 \pm 0.001
CIFAR-100	Logloss	0.798 \pm 0.007	0.300 \pm 0.002	78.4% \pm 0.3	0.020 \pm 0.002	0.020 \pm 0.002
	Brier score	0.803 \pm 0.003	0.298 \pm 0.001	78.8% \pm 0.1	0.021 \pm 0.002	0.020 \pm 0.001
	Accuracy	0.791 \pm 0.011	0.300 \pm 0.002	78.6% \pm 0.2	0.020 \pm 0.003	0.019 \pm 0.002
	TS-refinement	0.771 \pm 0.004	0.298 \pm 0.002	78.5% \pm 0.2	0.016 \pm 0.002	0.016 \pm 0.001
SVHN	Logloss	0.109 \pm 0.002	0.043 \pm 0.001	97.3% \pm 0.1	0.007 \pm 0.001	0.008 \pm 0.001
	Brier score	0.110 \pm 0.003	0.042 \pm 0.001	97.3% \pm 0.1	0.007 \pm 0.001	0.008 \pm 0.001
	Accuracy	0.112 \pm 0.002	0.042 \pm 0.001	97.3% \pm 0.1	0.008 \pm 0.001	0.009 \pm 0.001
	TS-refinement	0.109 \pm 0.001	0.042 \pm 0.000	97.3% \pm 0.1	0.007 \pm 0.001	0.008 \pm 0.001

Table F.2: Benchmark results for WideResNet. We plot means obtained over the 10 runs and 95% confidence intervals computed using the t-distribution. Stopping metrics are evaluated on the validation set (10% of training data). All metrics are reported for the best model as selected by the corresponding stopping metric, after TS (fitted using the validation set).

G. Tabular experiments

In the following, we provide more details and analyses for our tabular experiments. The experiments took around 40 hours to run on a workstation with a 32-core AMD Threadripper PRO 3975WX CPU and four NVidia RTX 3090 GPUs. The benchmark code is available at github.com/dholzmueller/pytabkit.

G.1. Dataset size dependency

Figure G.1 shows how the relative performance of refinement-based stopping vs logloss stopping depends on the dataset size. While the situation for small datasets is very noisy, for larger datasets the deterioration in the worst case is much less severe than the improvements in the best case. The advantages of TS-refinement become apparent at roughly 10K samples, which corresponds to a validation set size of 1,600. For XGB and MLP, there is one large outlier dataset where refinement-based stopping and logloss stopping both achieve low loss but the loss ratio is high.

G.2. Other stopping metrics

In Figure G.2, we show results for more stopping metrics like AUROC, Brier loss, Brier loss after temperature scaling, and a 5-fold cross-validation version of TS-Refinement from Appendix E. TS-Refinement and its more expensive cross-validation version perform best. Out of the other metrics, Brier loss before or after temperature scaling performs comparably to logloss, while AUROC performs worse than logloss for RealMLP.

G.3. Effect on other metrics

Figure G.3 shows that tuning TS-Refinement can, on average, improve downstream accuracy compared to tuning logloss, and sometimes even compared to tuning accuracy directly. The same holds for AUROC in Figure G.4, where tuning accuracy often performs very badly. Performing temperature scaling does not affect downstream accuracy, but can affect downstream AUROC on multiclass datasets.

G.4. Stopping times

Figure G.5 shows the best epochs or iterations found for different metrics for the models with default parameters. We can see several tendencies across models:

- Logloss stops first on average.
- Brier loss stops later than logloss, also when considering the loss after temperature scaling.
- Loss after temperature scaling stops later than loss before temperature scaling.
- Accuracy stops late and AUROC somewhere in the middle.

G.5. Methods

From a single training of a method, we extract results for the best epoch (for NNs) or iteration (for XGBoost) with respect to all considered metrics. To achieve this, we always train for the maximum number of epochs/iterations and do not stop the training early based on one of the metrics.

Default parameters For the MLP, we slightly simplify the default parameters of (Gorishniy et al., 2021) as shown in Table G.3. For XGBoost, we take the library default parameters. For RealMLP, we take the default parameters from Holz Müller et al. (2024) but deactivate label smoothing since it causes the loss to be non-proper.

Hyperparameter tuning For hyperparameter tuning, we employ 30 steps of random search, comparable to McElfresh et al. (2024). Using random search allows us to train the 30 random models once and then pick the best one for each metric. For the MLP, we choose a small search space, shown in Table G.4 to cover the setting of a simple baseline. For XGBoost, we choose a typical, relatively large search space, shown in Table G.1. For RealMLP, we slightly modify the original search space from Holz Müller et al. (2024).

G.6. Datasets

We take the datasets from Ye et al. (2024) and apply the following modifications:

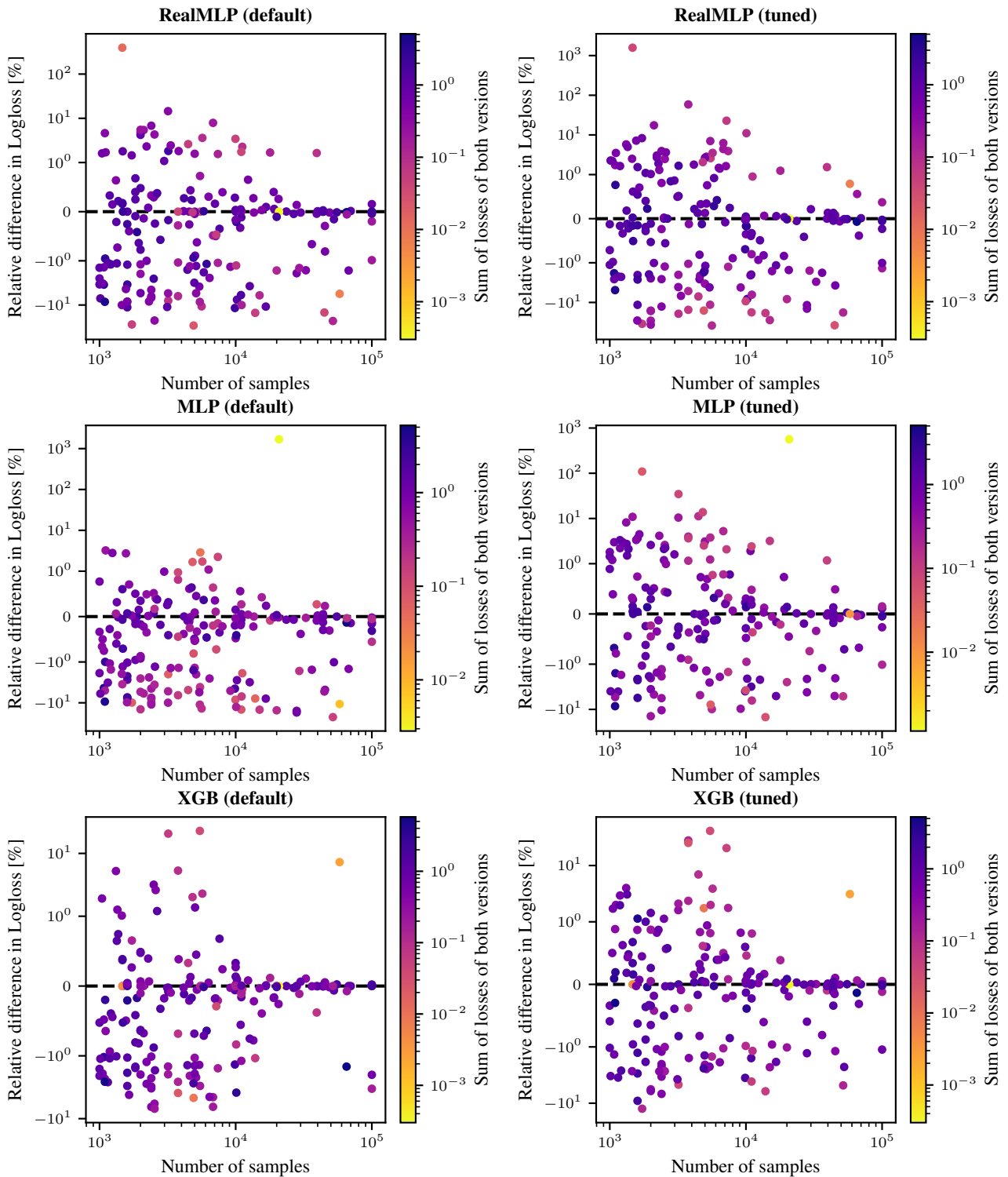


Figure G.1: **Relative differences in logloss of using TS-Refinement vs. Logloss for selecting the best epoch and hyperparameters.** Each method applies temperature scaling on the final model. Each dot represents one dataset. Values below zero mean that TS-refinement performs better. A light color indicates datasets where methods achieve very low loss.

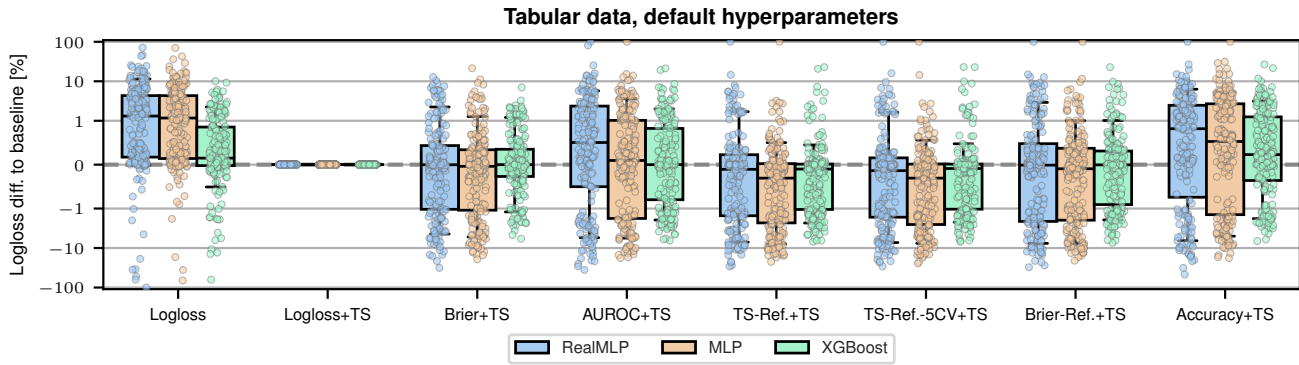


Figure G.2: **Relative differences in logloss for different stopping methods compared to Logloss+TS.** Brier-Ref. refers to Brier loss after temperature scaling. AUROC uses the one-vs-rest version for multiclass datasets. TS-Ref.-5CV is the metric from Appendix E computing the out-of-fold loss after temperature scaling in a five-fold crossvalidation setup. Methods labeled “+TS” use temperature scaling on the final model. Each dot represents one dataset from Ye et al. (2024), using only the 65 datasets with at least 10K samples. Percentages are clipped to $[-100, 100]$. Box-plots show the 10%, 25%, 50%, 75%, and 90% quantiles.

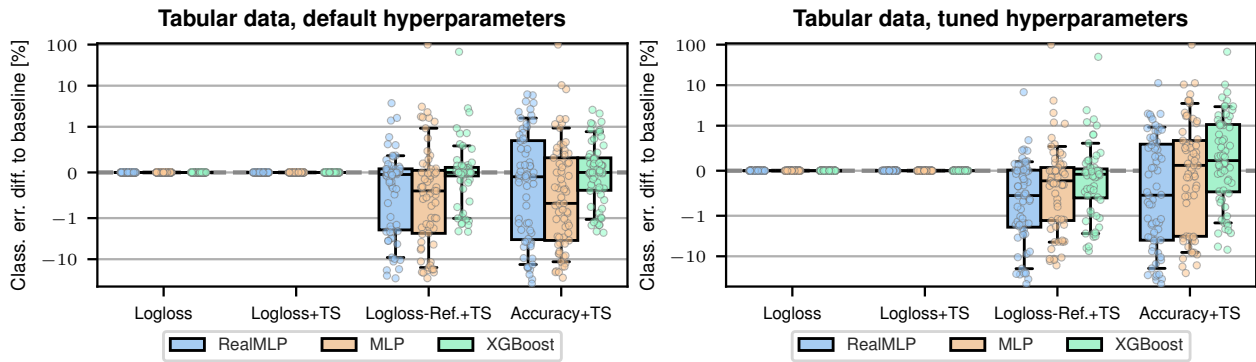


Figure G.3: **Differences in downstream classification error between logloss + TS and other procedures on tabular datasets.** Each dot represents one dataset from Ye et al. (2024), using only the 65 datasets with at least 10K samples. Percentages are clipped to $[-100, 100]$. Box-plots show the 10%, 25%, 50%, 75%, and 90% quantiles.

- Samples that contain missing values in numerical features are removed since not all methods natively support the handling of these values.
- Datasets that contain less than 1K samples after the previous steps are removed. The following datasets are removed: analcatdata.authorship, Pima.Indians.Diabetes.Database, vehicle, mice.protein.expression, and eucalyptus. The latter two datasets contained samples with missing numerical features.
- Datasets with more than 100K samples are subsampled to 100K samples.

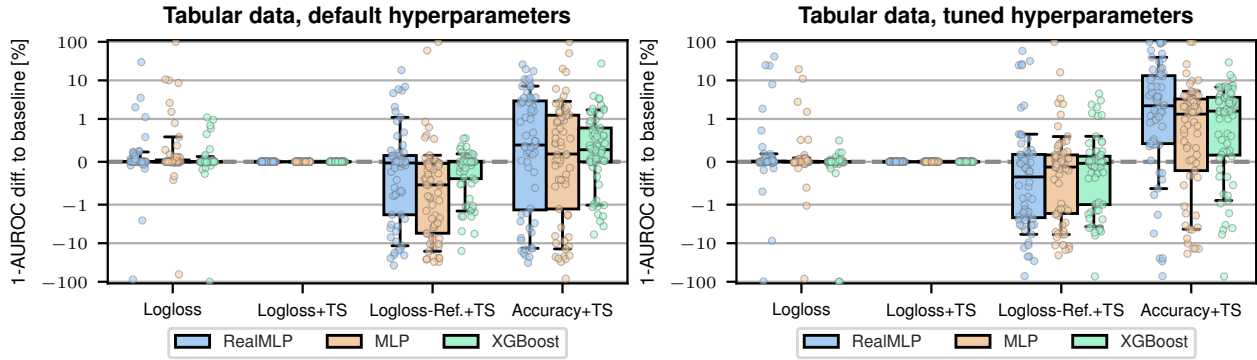


Figure G.4: Differences in downstream *AUROC* (one-vs-rest for multiclass datasets) between logloss + TS and other procedures on tabular datasets. Each dot represents one dataset from Ye et al. (2024), using only the 65 datasets with at least 10K samples. Percentages are clipped to $[-100, 100]$. Box-plots show the 10%, 25%, 50%, 75%, and 90% quantiles.

Table G.1: Hyperparameter search space for XGBoost, adapted from Grinsztajn et al. (2022). We use the `hist` method, which is the new default in XGBoost 2.0 and supports native handling of categorical values, while the old `auto` method selection is not available in XGBoost 2.0. We disable early stopping as we want to select the best epoch for different metrics in the same training run. Some search spaces are adapted based on previous experiences.

Hyperparameter	Distribution
<code>tree_method</code>	<code>hist</code>
<code>n_estimators</code>	1000
<code>early_stopping_rounds</code>	1000
<code>max_depth</code>	<code>UniformInt[1, 11]</code>
<code>learning_rate</code>	<code>LogUniform[1e-3, 0.7]</code>
<code>subsample</code>	<code>Uniform[0.5, 1]</code>
<code>colsample_bytree</code>	<code>Uniform[0.5, 1]</code>
<code>colsample_bylevel</code>	<code>Uniform[0.5, 1]</code>
<code>min_child_weight</code>	<code>LogUniformInt[1e-5, 100]</code>
<code>alpha</code>	<code>LogUniform[1e-5, 5]</code>
<code>lambda</code>	<code>LogUniform[1e-5, 5]</code>
<code>gamma</code>	<code>LogUniform[1e-5, 5]</code>

Table G.2: Hyperparameter search space for RealMLP, adapted from Holzmüller et al. (2024). Compared to the original search space, we make the option without label smoothing more likely since it optimizes a proper loss, and we insert a third option for weight decay.

Hyperparameter	Distribution
Num. embedding type	<code>Choice([None, PBLD, PL, PLR])</code>
Use scaling layer	<code>Choice([True, False], p=[0.6, 0.4])</code>
Learning rate	<code>LogUniform([2e-2, 3e-1])</code>
Dropout prob.	<code>Choice([0.0, 0.15, 0.3], p=[0.3, 0.5, 0.2])</code>
Activation fct.	<code>Choice([ReLU, SELU, Mish])</code>
Hidden layer sizes	<code>Choice([[256, 256, 256], [64, 64, 64, 64, 64], [512]], p=[0.6, 0.2, 0.2])</code>
Weight decay	<code>Choice([0.0, 2e-3, 2e-2])</code>
Num. emb. init std.	<code>LogUniform([0.05, 0.5])</code>
Label smoothing ϵ	<code>Choice([0.0, 0.1])</code>

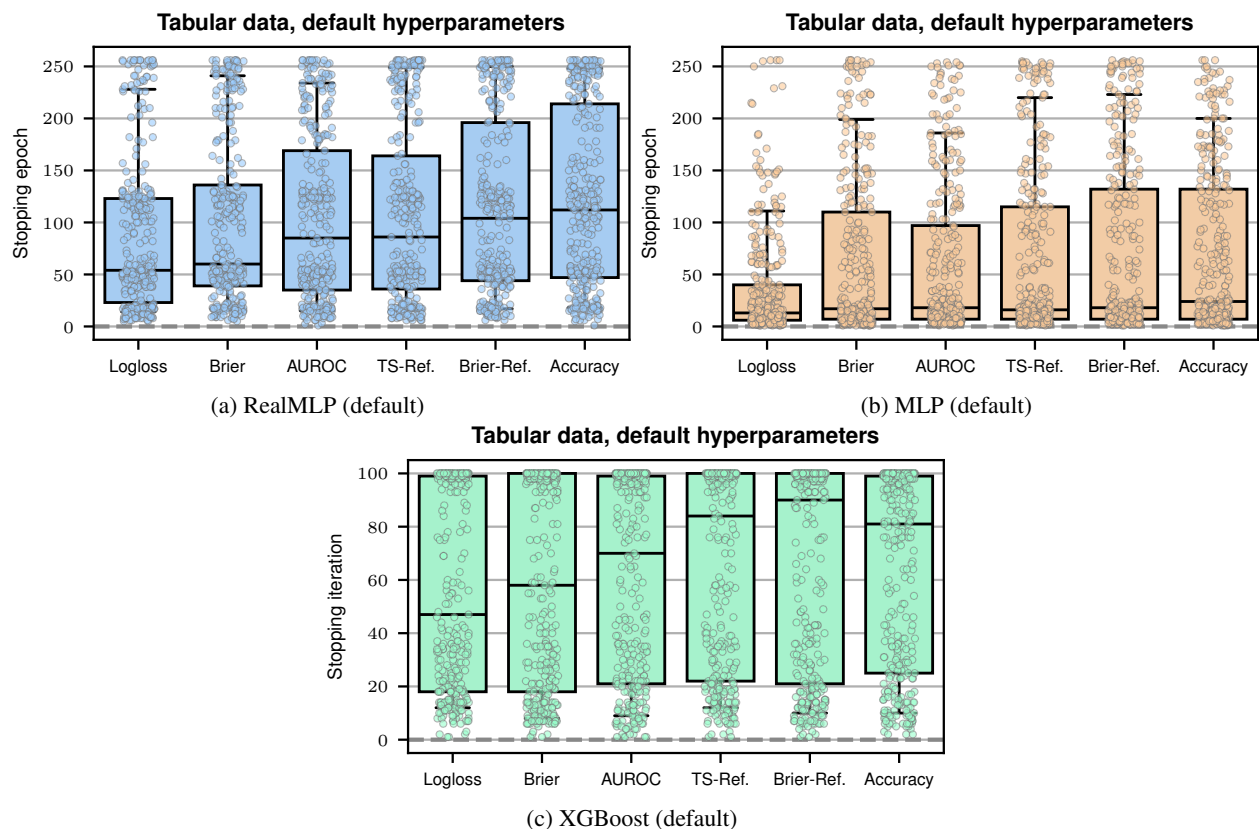


Figure G.5: **Best epochs/iterations in default models for different stopping metrics.** Each point represents one model trained on one of five training-validation splits on one of the 65 datasets with at least 10K samples. Brier-Ref. refers to Brier loss after temperature scaling. AUROC uses the one-vs-rest version for multiclass datasets. The multiple clusters in the RealMLP stopping epochs are likely due to the use of a multi-cycle loss schedule.

Table G.3: Default hyperparameters for MLP, adapted from (Gorishniy et al., 2021).

Hyperparameter	Distribution
Number of layers	4
Hidden size	256
Activation function	ReLU
Learning rate	1e-3
Dropout	0.0
Weight decay	0.0
Optimizer	AdamW
Preprocessing	Quantile transform + one-hot encoding
Batch size	256
Number of epochs	256
Learning rate schedule	constant

Table G.4: Hyperparameter search space for MLP.

Hyperparameter	Distribution
Learning rate	LogUniform[1e-4, 1e-2]
Dropout	Choice([0.0, 0.1, 0.2, 0.3])
Weight decay	Choice([0.0, 1e-5, 1e-4, 1e-3])